Date: 23/03/2023

Multicellular and Population Models of Neuroblastoma to Improve Multi-Modal Therapy

Dr Kenneth Y. Wertheim (they/them)

Also known as 11250205

k.y.wertheim@hull.ac.uk

Introduction

1. **Neuroblastoma.**
2. PRIMAGE.

Neuroblastoma

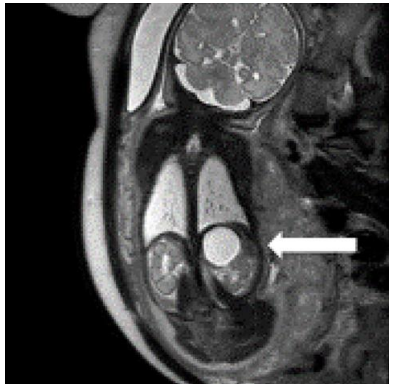

Louis, Chrystal U., and Jason M. Shohet. "Neuroblastoma: molecular pathogenesis and therapy." *Annual review of medicine* 66 (2015): 49.

1. Adrenal medulla is the usual primary site.

2. Most common extracranial solid tumour in children.

3. 15 % of cancer-related deaths in this population.

Neuroblastoma

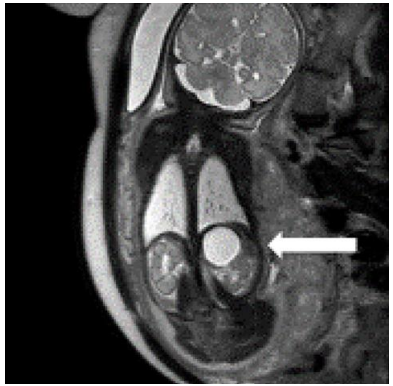

Louis, Chrystal U., and Jason M. Shohet. "Neuroblastoma: molecular pathogenesis and therapy." *Annual review of medicine* 66 (2015): 49.

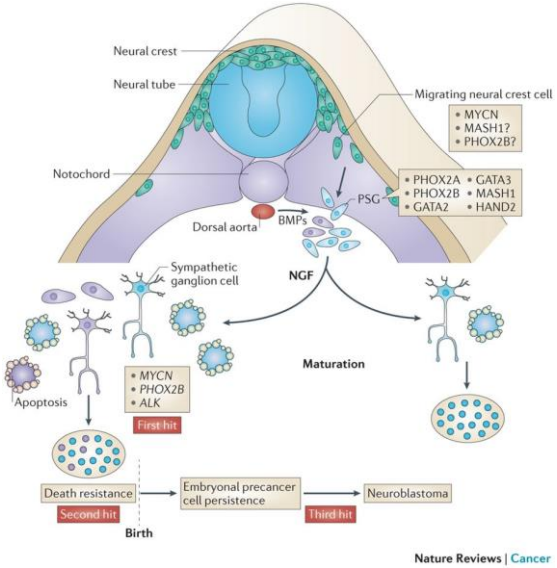

Marshall, Glenn M., et al. "The prenatal origins of cancer." *Nature Reviews Cancer* 14.4 (2014): 277-289.

1. Adrenal medulla is the usual primary site.

2. Most common extracranial solid tumour in children.

3. 15 % of cancer-related deaths in this population.

1. Neural crest, transient in the embryo.

2. Differentiate into different cell types.

3. Sympathetic nervous system.

4. MYCN amplification and ALK activation turn them into neuroblastoma cancer cells.

Neuroblastoma

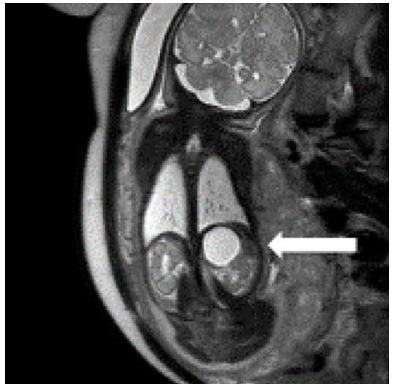

Louis, Chrystal U., and Jason M. Shohet. "Neuroblastoma: molecular pathogenesis and therapy." *Annual review of medicine* 66 (2015): 49.

1. Adrenal medulla is the usual primary site.

2. Most common extracranial solid tumour in children.

3. 15 % of cancer-related deaths in this population.

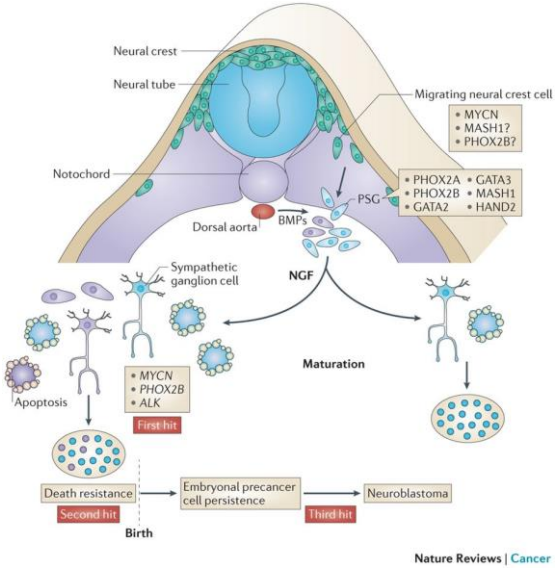

Marshall, Glenn M., et al. "The prenatal origins of cancer." *Nature Reviews Cancer* 14.4 (2014): 277-289.

1. Neural crest, transient in the embryo.

2. Differentiate into different cell types.

3. Sympathetic nervous system.

4. MYCN amplification and ALK activation turn them into neuroblastoma cancer cells.

INRG Stage	Age (months)	Histologic Category	Grade of Tumor Differentiation	*MYCN*	11q Aberration	Ploidy	Pretreatment Risk Group
L1/L2		GN maturing; GNB intermixed					A Very low
L1		Any, except GN maturing or GNB intermixed		NA			B Very low
				Amp			K High
L2	< 18	Any, except GN maturing or GNB intermixed		NA	No		D Low
					Yes		G Intermediate
	≥ 18	GNB nodular; neuroblastoma	Differentiating	NA	No		E Low
					Yes		H Intermediate
			Poorly differentiated or undifferentiated	NA			
				Amp			N High
M	< 18			NA		Hyperdiploid	F Low
	< 12			NA		Diploid	I Intermediate
	12 to < 18			NA		Diploid	J Intermediate
	< 18			Amp			O High
	≥ 18						P High
MS	< 18			NA	No		C Very low
					Yes		Q High
				Amp			R High

Sokol, Elizabeth, and Ami V. Desai. "The evolution of risk classification for neuroblastoma." *Children* 6.2 (2019): 27.

1. Low risk, spontaneous regression.

2. High risk, 50 % relapse.

3. MYCN amplification is a bad sign.

Neuroblastoma

Current standard:
multi-modal therapy.

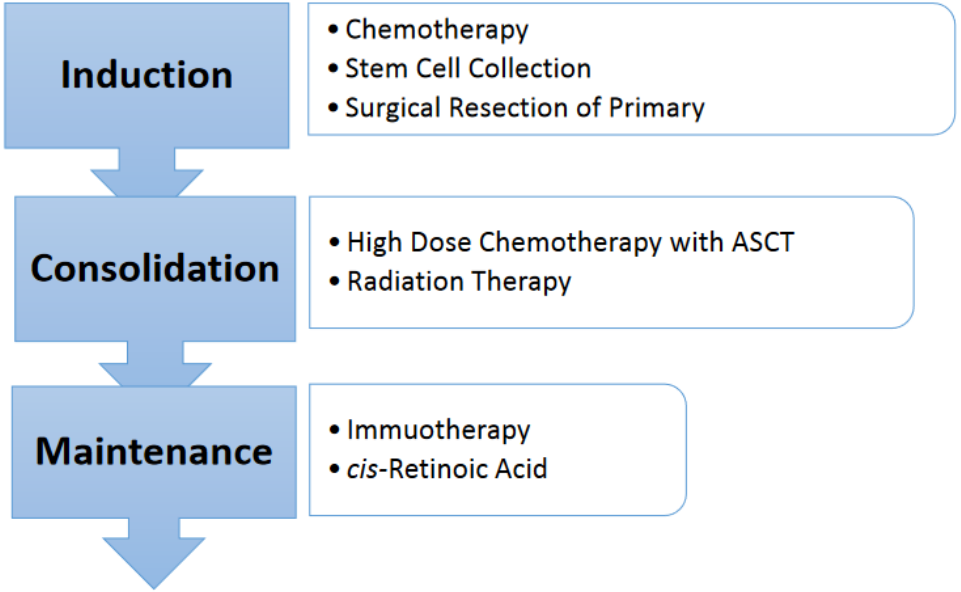

Smith, Valeria, and Jennifer Foster. "High-risk neuroblastoma treatment review." *Children* 5.9 (2018): 114.

PRIMAGE project: predictive *in silico* multiscale analytics to support childhood cancer personalised evaluation empowered by imaging biomarkers

Luis Martí-Bonmatí[1*], Ángel Alberich-Bayarri[2], Ruth Ladenstein[3], Ignacio Blanquer[4], J. Damian Segrelles[4], Leonor Cerdá-Alberich[5], Polyxeni Gkontra[5], Barbara Hero[6], J. M. García-Aznar[7,8], Daniel Keim[9], Wolfgang Jentner[9], Karine Seymour[10], Ana Jiménez-Pastor[2], Ismael González-Valverde[2], Blanca Martínez de las Heras[11], Samira Essiaf[12], Dawn Walker[13], Michel Rochette[14], Marian Bubak[15], Jordi Mestres[16], Marco Viceconti[17], Gracia Martí-Besa[5], Adela Cañete[11], Paul Richmond[13], Kenneth Y. Wertheim[13], Tomasz Gubala[15], Marek Kasztelnik[15], Jan Meizner[15], Piotr Nowakowski[15], Salvador Gilpérez[18], Amelia Suárez[18], Mario Aznar[18], Giuliana Restante[19] and Emanuele Neri[19]

Decision support system for the clinical management of malignant solid tumours.

Introduction

1. Neuroblastoma.
2. **PRIMAGE.**

Primage

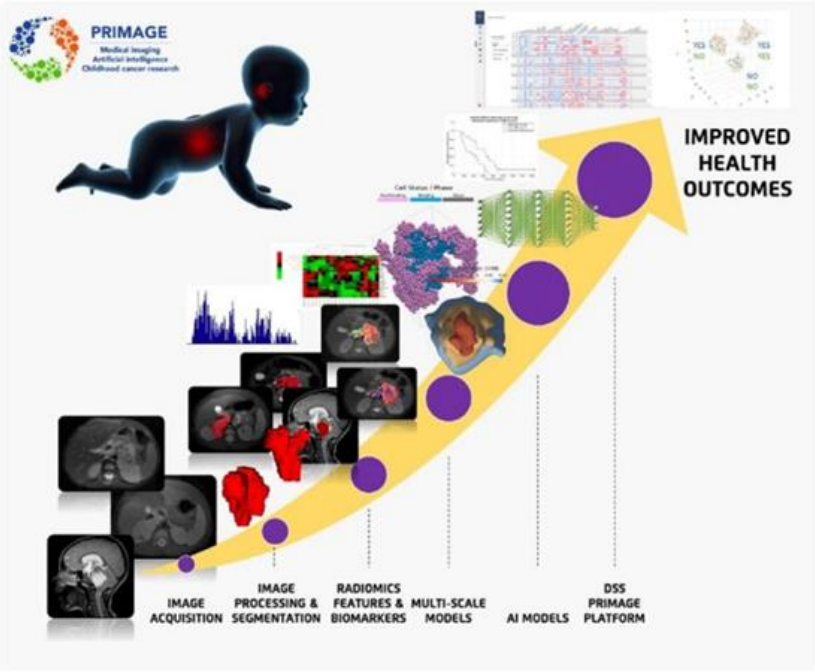

Decision support system for the clinical management of malignant solid tumours.

1. Image acquisition, processing, and segmentation.
2. Integrate radiomic features with other biomarkers, such as mutations and histology.
3. **Multiscale models: organ/tumour, tissue, and intracellular.**
4. Machine learning techniques extract insights from simulation results.

Martí-Bonmatí, Luis, et al. "PRIMAGE project: predictive in silico multiscale analytics to support childhood cancer personalised evaluation empowered by imaging biomarkers." *European radiology experimental* 4.1 (2020): 1-11.

Primage

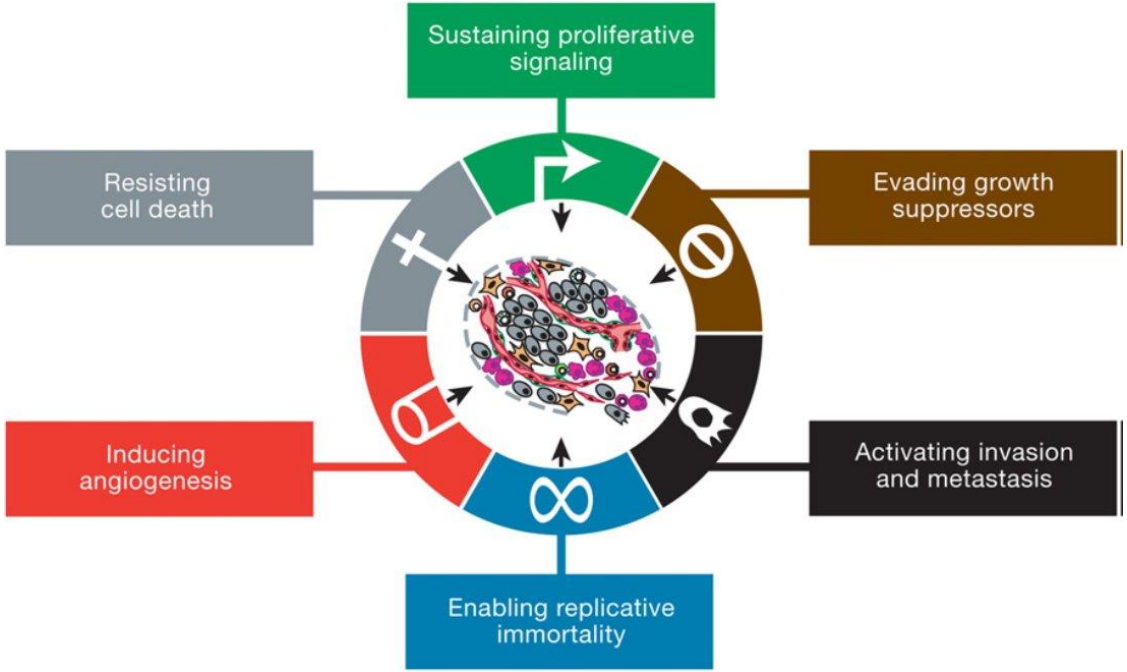

Hanahan, Douglas, and Robert A. Weinberg. "Hallmarks of cancer: the next generation." *cell* 144.5 (2011): 646-674.

Primage

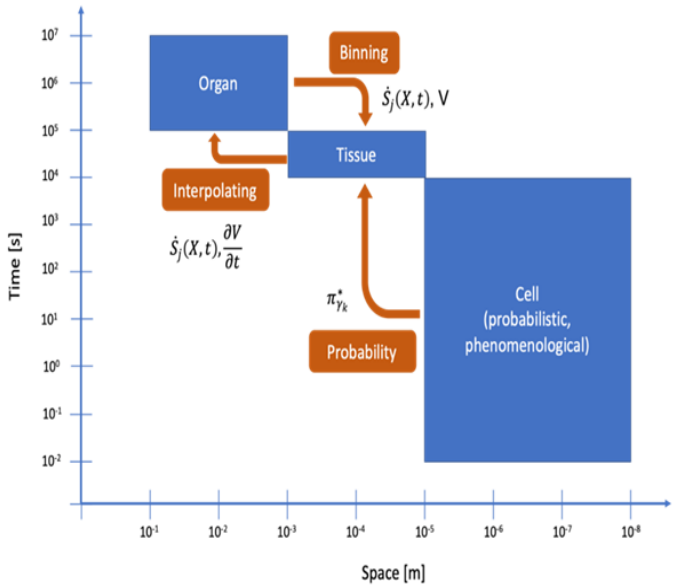

de Melo Quintela, B., Hervás-Raluy, S., Garcia-Aznar, J.M., Walker, D., Wertheim, K.Y., and Viceconti, M., 2021. A Theoretical Analysis of the Scale Separation in a Model to Predict Solid Tumour Growth. *Journal of Theoretical Biology*. Manuscript under review and available upon request.

Cannot describe biological phenomena spanning **nine orders of magnitude** in a single-scale model.

1. Experimental resolutions.
2. Model complexity.
3. Computational costs.

ALMA MATER STUDIORUM
UNIVERSITÀ DI BOLOGNA

Primage

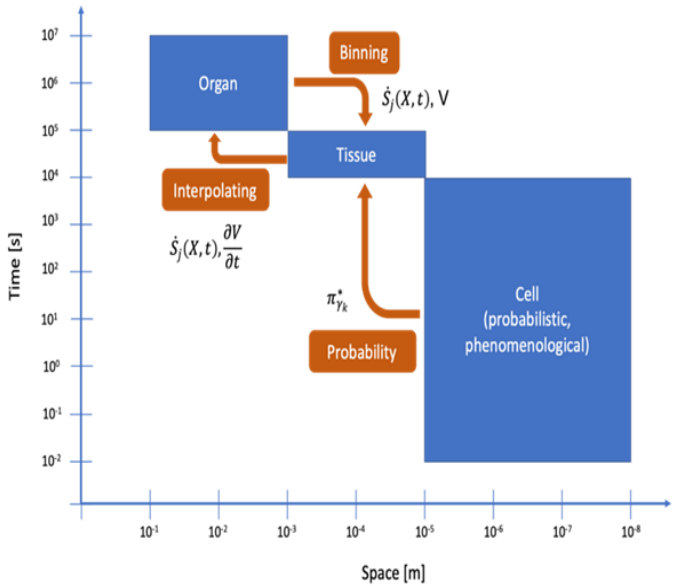

de Melo Quintela, B., Hervás-Raluy, S., Garcia-Aznar, J.M., Walker, D., Wertheim, K.Y., and Viceconti, M., 2021. A Theoretical Analysis of the Scale Separation in a Model to Predict Solid Tumour Growth. *Journal of Theoretical Biology*. Manuscript under review and available upon request.

Universidad Zaragoza

Chemotargets

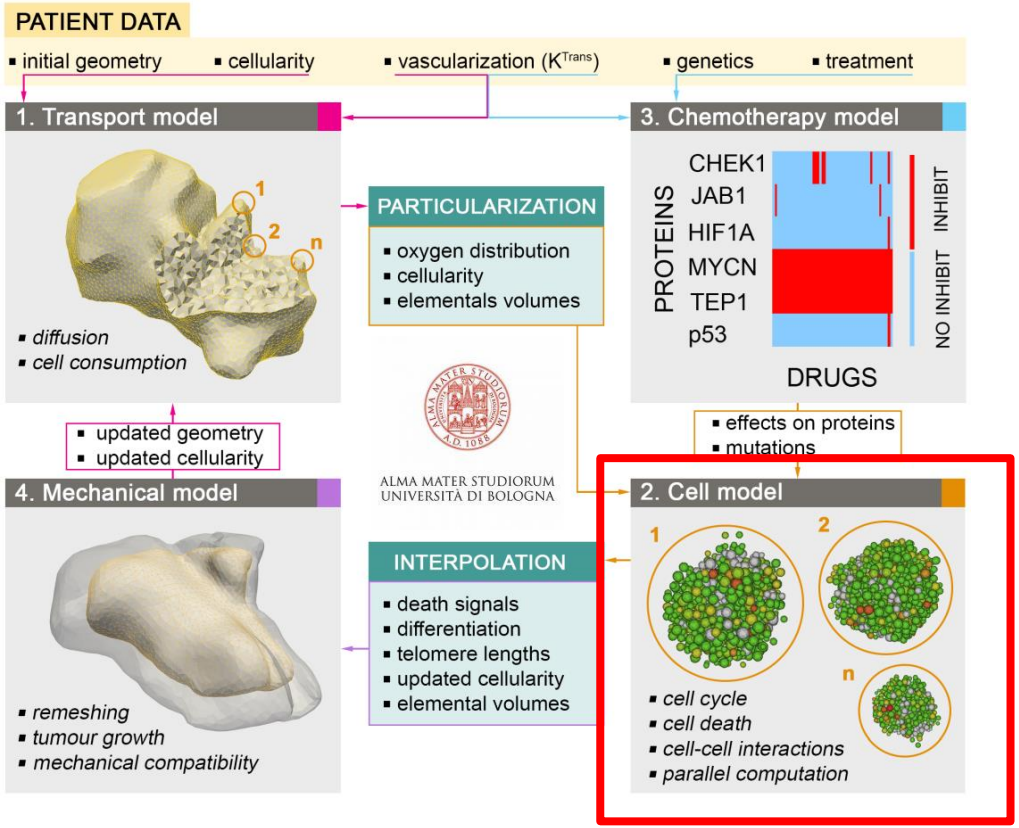

ALMA MATER STUDIORUM UNIVERSITÀ DI BOLOGNA

Universidad Zaragoza

University of Sheffield

Multicellular model

1. **Model structure.**
2. Model calibration.
3. Clonal competition.
4. p53 and p73.
5. Targeted therapies.
6. Surrogate modelling.

Model structure

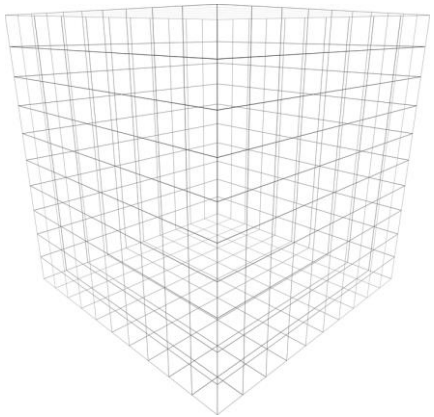

Continuous automaton to voxelate the microenvironment.

1. Spatial distributions of cells and extracellular matrix.

2. Concentration dynamics of drugs and nutrients (uniform).

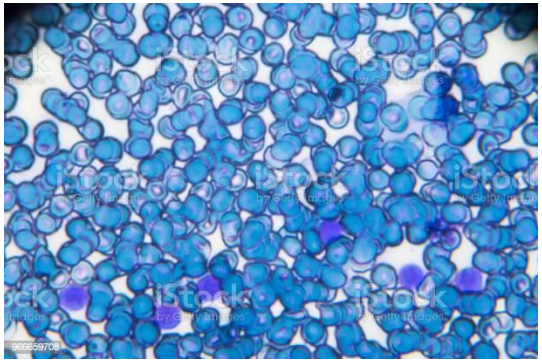

Discrete agents.

1. Neuroblastoma and Schwann cells.
2. Cell cycling and death.

Agent attributes.

1. Mutations.
2. DNA status.
3. Gene expression levels.

Model structure

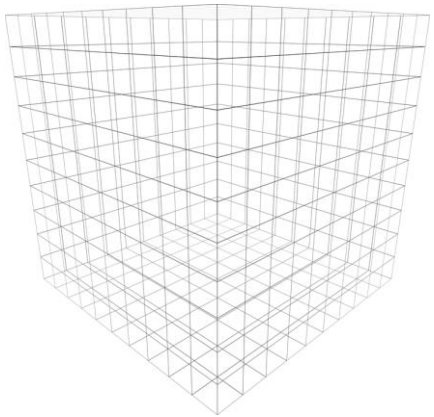

Continuous automaton to voxelate the microenvironment.

1. Spatial distributions of cells and extracellular matrix.

2. Concentration dynamics of drugs and nutrients (uniform).

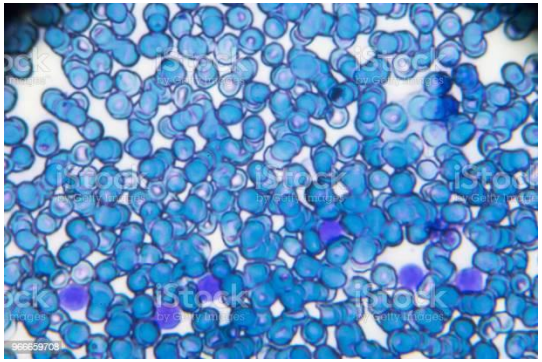

Discrete agents.

1. Neuroblastoma and Schwann cells.
2. Cell cycling and death.

Agent attributes.

1. Mutations.
2. DNA status.
3. **Gene expression levels.**

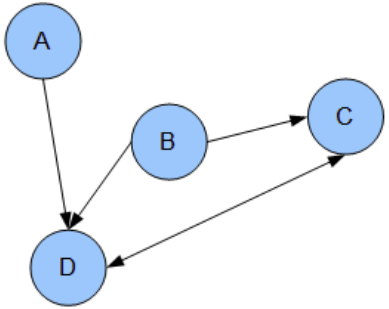

20 gene products.Telomerase, ALT, MYCN, MAPK/RAS pathway, JAB1, CHK1, CDS1, CDC25C, ID2, IAP2, HIF, BNIP3, VEGF, p53, p73, p21, p27, Bcl-2/Bcl-xL, BAK/BAX, and CAS.

Model structure

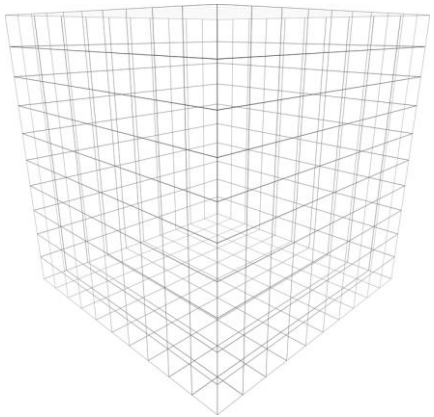

Continuous automaton to voxelate the microenvironment.

1. Spatial distributions of cells and extracellular matrix.

2. Concentration dynamics of drugs and nutrients (uniform).

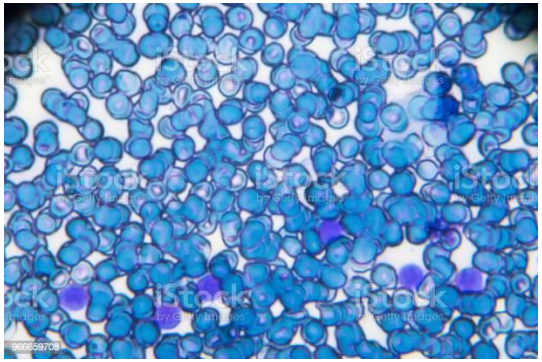

Discrete agents.

1. Neuroblastoma and Schwann cells.
2. Cell cycling and death.

Agent attributes.

1. Mutations.
2. DNA status.
3. Gene expression levels.

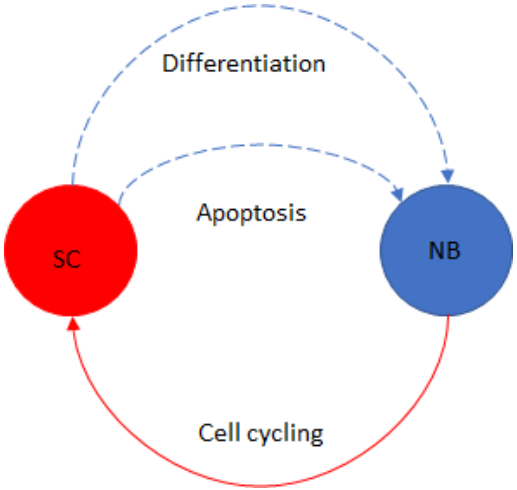

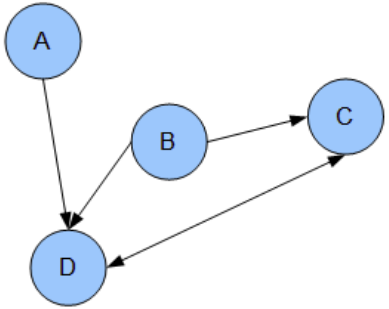

20 gene products.Telomerase, ALT, MYCN, MAPK/RAS pathway, JAB1, CHK1, CDS1, CDC25C, ID2, IAP2, HIF, BNIP3, VEGF, p53, p73, p21, p27, Bcl-2/Bcl-xL, BAK/BAX, and CAS.

Model structure

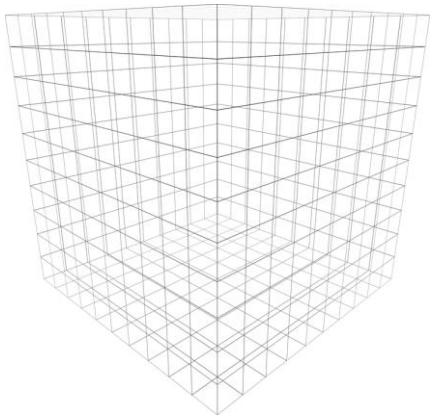

Continuous automaton to voxelate the microenvironment.

1. Spatial distributions of cells and extracellular matrix.

2. Concentration dynamics of drugs and nutrients (uniform).

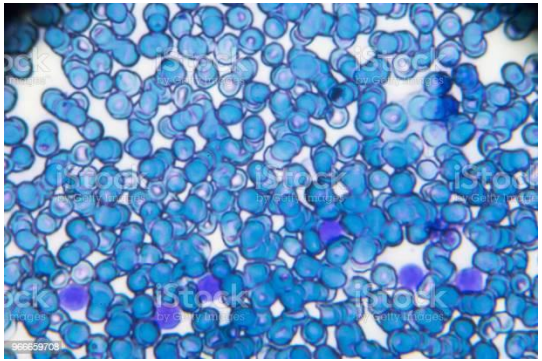

Discrete agents.

1. Neuroblastoma and Schwann cells.
2. Cell cycling and death.

Agent attributes.

1. Mutations.
2. DNA status.
3. Gene expression levels.

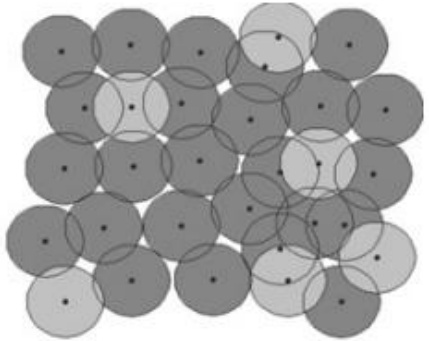

Centre-based mechanical model.

1. Resolve agent-agent overlap and contact inhibition.

2. Linear force law.

3. Equation of motion.

Model structure

Stochastic simulation algorithm

1. Each agent senses the microenvironment and its neighbouring agents, modifies its behaviour, and updates its attributes.

2. Resolve agent-agent overlap using the mechanical model.

3. Modify the microenvironment by considering the agents collectively.

4. Back to step 1.

A series of Bernoulli trials. For example, is the MAPK/RAS pathway active?

Multicellular model

1. Model structure.
2. **Model calibration.**
3. Clonal competition.
4. p53 and p73.
5. Targeted therapies.
6. Surrogate modelling.

Model calibration

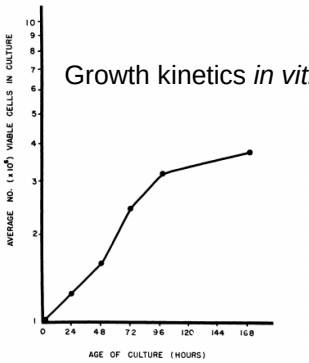

Growth kinetics *in vitro*.

Tumilowicz, Joseph J., et al. "Definition of a continuous human cell line derived from neuroblastoma." *Cancer research* 30.8 (1970): 2110-2118.

	Three-stage fit	95% CI	Direct fit	95% CI
Maximum oxygen consumption rate, q_{max} (mmHg · s^{-1})	17.5	15.3–25.1	16.3	15.3–17.9
P_{O_2} for 50% drop in consumption, $P_{50,q}$ (mmHg)	2.7	0.0–12.5	1.6	1.2–2.1
Maximum misonidazole binding rate, $k_{b,0}$ ($\times 10^{-4}$ s^{-1})	4.5	3.9–4.9	4.4	2.5–5.3
P_{O_2} for 50% drop in binding, $P_{50,b}$ (mmHg)	1.4	0.3–2.6	1.4	1.1–2.5
P_{O_2} for 50% necrosis, $P_{50,n}$ (mmHg)	1.2	0.1–4.9	1.0	0.4–1.2

Warren, Daniel R., and Mike Partridge. "The role of necrosis, acute hypoxia and chronic hypoxia in 18F-FMISO PET image contrast: a computational modelling study." *Physics in Medicine & Biology* 61.24 (2016): 8596.

Extent of necrosis during hypoxia *in vitro*.

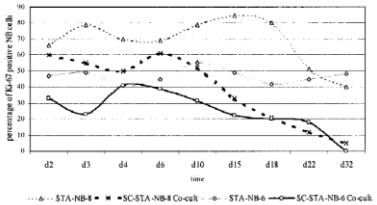

Ambros, Ingeborg M., et al. "Neuroblastoma cells provoke Schwann cell proliferation in vitro." *Medical and Pediatric Oncology: The Official Journal of SIOP—International Society of Pediatric Oncology (Societé Internationale d'Oncologie Pédiatrique)* 36.1 (2001): 163-168.

Interactions between neuroblastoma and Schwann cells *in vitro*.

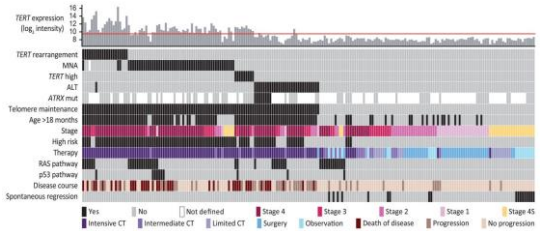

Ackermann, Sandra, et al. "A mechanistic classification of clinical phenotypes in neuroblastoma." *Science* 362.6419 (2018): 1165-1170.

Clinical outcomes associated with different mutations.

Model calibration

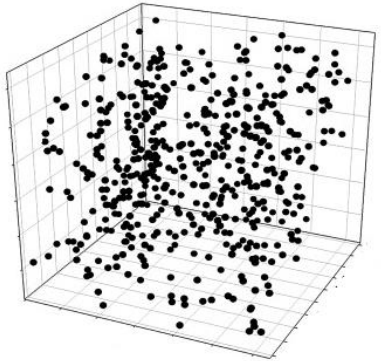

Latin hypercube sampling.

1. 3000 combinations of 20 fitting parameters.

2. Minimised differences between simulation results and *in vitro* data.

3. Refined calibrated parameters for *in vivo* use.

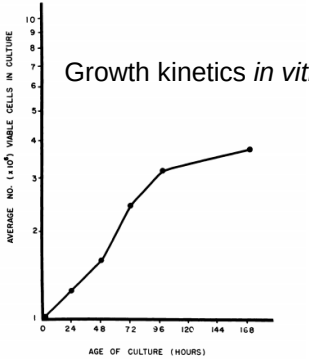

Growth kinetics *in vitro*.

Tumilowicz, Joseph J., et al. "Definition of a continuous human cell line derived from neuroblastoma." *Cancer research* 30.8 (1970): 2110-2118.

	Three-stage fit	95% CI	Direct fit	95% CI
Maximum oxygen consumption rate, q_{max} (mmHg · s^{-1})	17.5	15.3–25.1	16.3	15.3–17.9
P_{O_2} for 50% drop in consumption, $P_{50,q}$ (mmHg)	2.7	0.0–12.5	1.6	1.2–2.1
Maximum misonidazole binding rate, $k_{b,0}$ ($\times 10^{-4}$ s^{-1})	4.5	3.9–4.9	4.4	2.5–5.3
P_{O_2} for 50% drop in binding, $P_{50,b}$ (mmHg)	1.4	0.3–2.6	1.4	1.1–2.5
P_{O_2} for 50% necrosis, $P_{50,n}$ (mmHg)	1.2	0.1–4.9	1.0	0.4–1.2

Warren, Daniel R., and Mike Partridge. "The role of necrosis, acute hypoxia and chronic hypoxia in 18F-FMISO PET image contrast: a computational modelling study." *Physics in Medicine & Biology* 61.24 (2016): 8596.

Extent of necrosis during hypoxia *in vitro*.

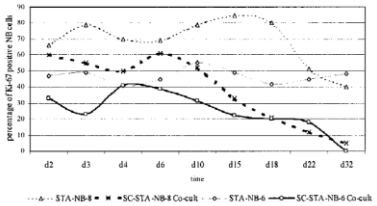

Ambros, Ingeborg M., et al. "Neuroblastoma cells provoke Schwann cell proliferation in vitro." *Medical and Pediatric Oncology: The Official Journal of SIOP—International Society of Pediatric Oncology (Societé Internationale d'Oncologie Pédiatrique)* 36.1 (2001): 163-168.

Interactions between neuroblastoma and Schwann cells *in vitro*.

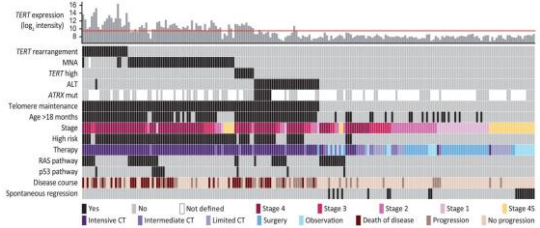

Ackermann, Sandra, et al. "A mechanistic classification of clinical phenotypes in neuroblastoma." *Science* 362.6419 (2018): 1165-1170.

Clinical outcomes associated with different mutations.

Model calibration

Squid Game. Created by Hwang Dong-hyuk, Netflix, 2021.

Index	MYCN_fn1	MAPK_RA	MAPK_RA	p53_fn	p73_fn	HIF_fn	P_cycle_si	P_DNA_da	P_DNA_c
677	0.277863	0.296396	0.081294	0.121137	0.168345	0.943243	0.529251	0.222474	0.99045
184	0.484521	0.518488	0.252074	0.676754	0.436464	0.658059	0.519606	0.614104	0.76648
2991	0.301635	0.87196	0.421385	0.797464	0.786514	0.234779	0.385223	0.219635	0.92531
825	0.892225	0.787593	0.215333	0.856983	0.718434	0.925868	0.25681	0.292857	0.98810
564	0.942648	0.377628	0.003161	0.19809	0.141042	0.59177	0.344412	0.772948	0.77149
1540	0.245592	0.997054	0.615927	0.603909	0.193378	0.311584	0.328683	0.659884	0.81446
2193	0.761934	0.675797	0.390508	0.893939	0.19777	0.760859	0.975454	0.337441	0.9600
1556	0.501221	0.879769	0.545846	0.085968	0.131161	0.13793	0.158815	0.126268	0.49899
675	0.69287	0.529858	0.232187	0.806742	0.69036	0.254842	0.541578	0.989668	0.97136
1892	0.547878	0.673346	0.579237	0.132174	0.816287	0.973364	0.553501	0.631952	0.87172
2307	0.832634	0.59399	0.204702	0.913315	0.654981	0.393086	0.472165	0.259098	0.90294
2198	0.485041	0.909258	0.218517	0.203592	0.042106	0.460479	0.623141	0.795116	0.95873
1106	0.815031	0.984735	0.400839	0.28017	0.267183	0.39705	0.947455	0.01568	0.10544

3000 candidates in study 1

1000 candidates in study 2

50 candidates in study 3

10 candidates in study 4

4 candidates in study 5

3 candidates in study 6

Model calibration

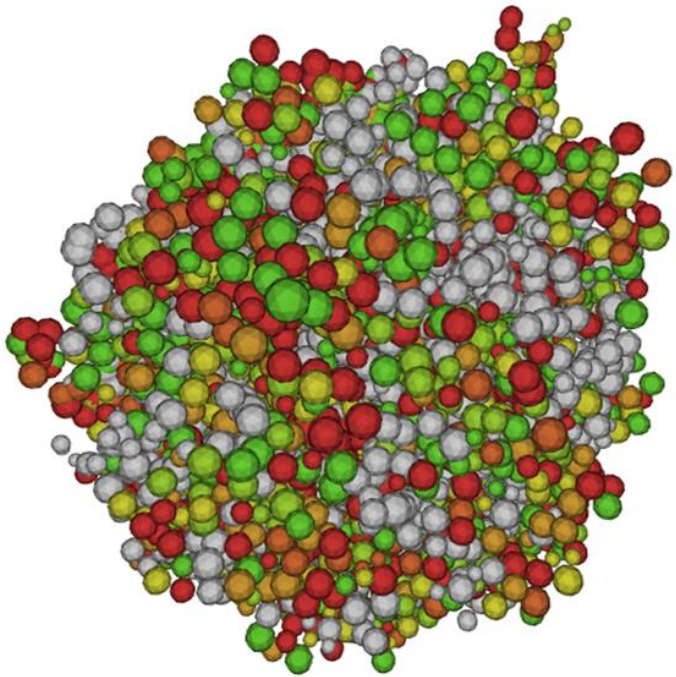

Costly simulations.
1. Millions of agents.
2. Four months in a patient's life.
3. Stochastic simulations.

Simulations on GPUs.

1. FLAMEGPU and FLAMEGPU2 were used to generate optimised CUDA code.

2. 3000 time steps took up to 10 minutes.

3. Calibration took 40 days in total.

Hardware: 2 TITAN V GPUs, 1 TITAN XP GPU, and 1 TITAN RTX GPU.

Multicellular model

1. Model structure.
2. Model calibration.
3. **Clonal competition.**
4. p53 and p73.
5. Targeted therapies.
6. Surrogate modelling.

Clonal competition

Clonal composition.
1. Four clones.
2. Each clone has six subclones.

Clones: MYCN amplification, TERT rearrangement, ATRX inactivation, and wild type.

Subclones: combinations of p53 inactivation and ALK activation.

Macroscopic features.
1. Oxygen level.
2. Abundance of Schwann cells.

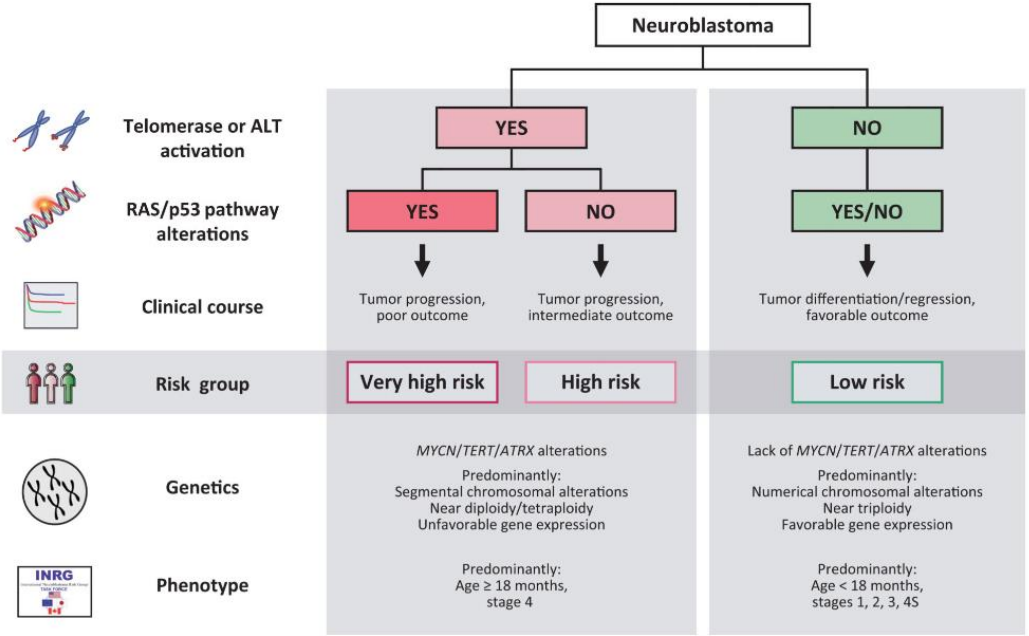

Ackermann, Sandra, et al. "A mechanistic classification of clinical phenotypes in neuroblastoma." *Science* 362.6419 (2018): 1165-1170.

Created 1200 virtual tumours with arbitrary clonal compositions and macroscopic features.

Clonal competition

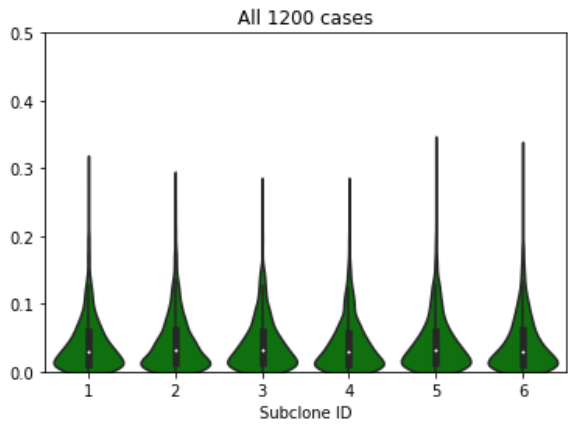

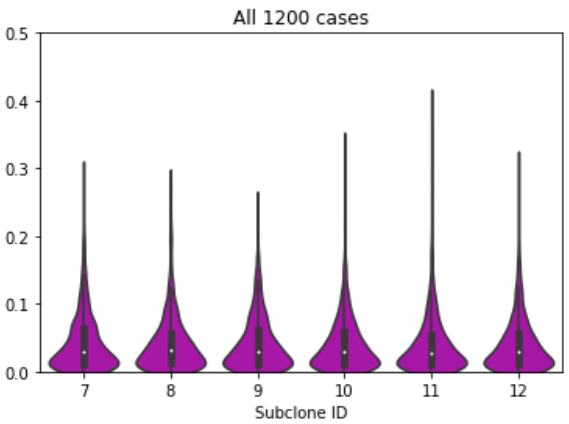

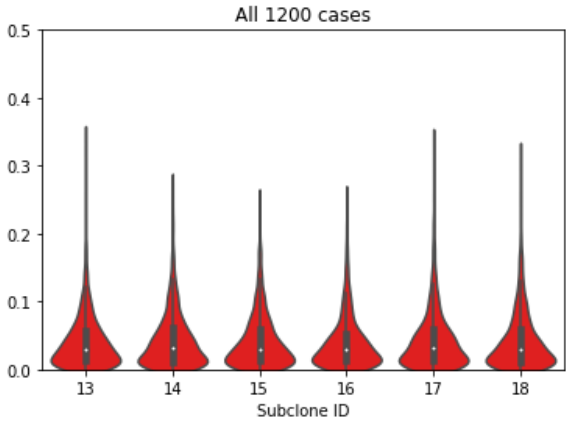

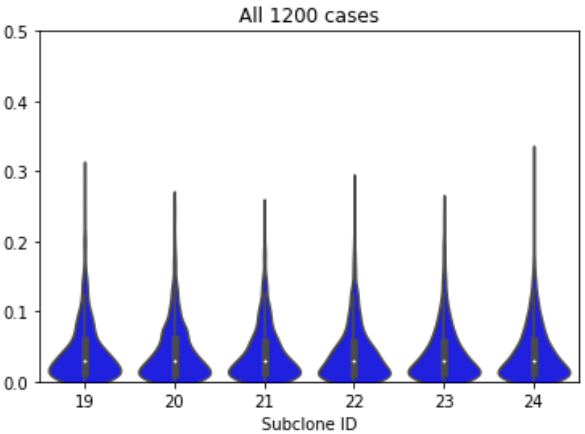

All 1200 tumours (control).

Input space.
1. Macroscopic features (left).
2. Initial clone sizes (right).

Clonal competition

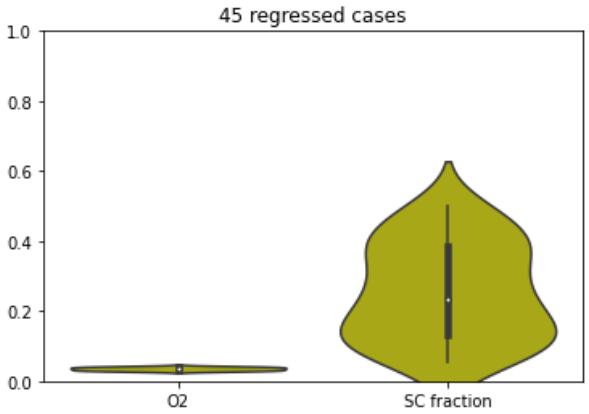

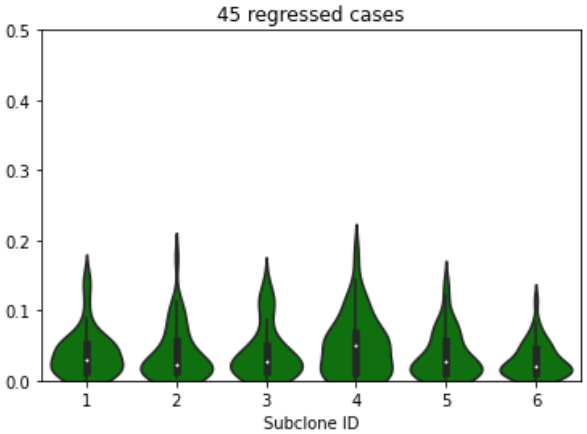

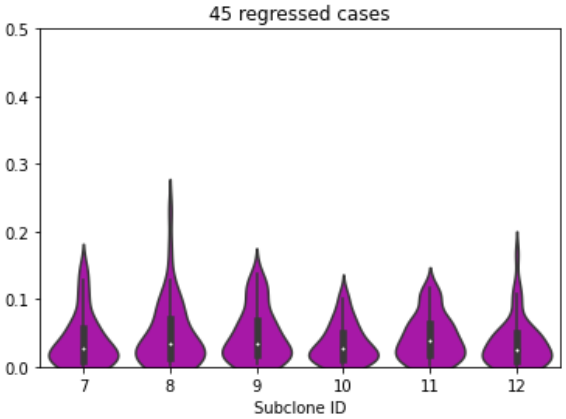

45 regressed cases.

Input space.
1. Hypoxia (left).
2. Uniform initial clone sizes (right).

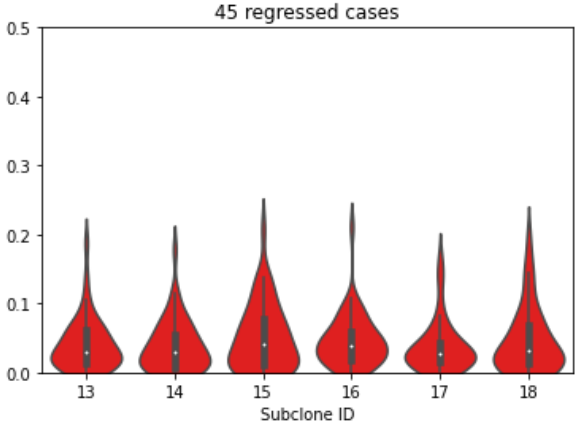

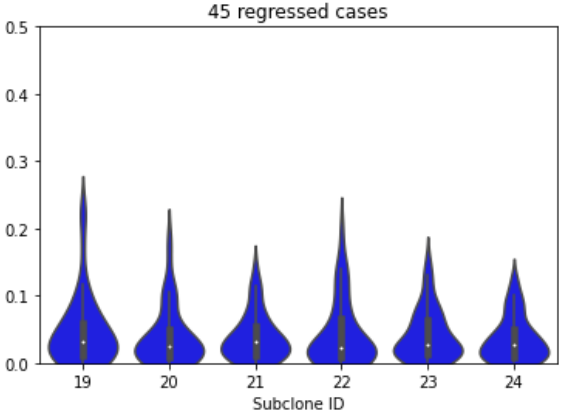

Clonal competition

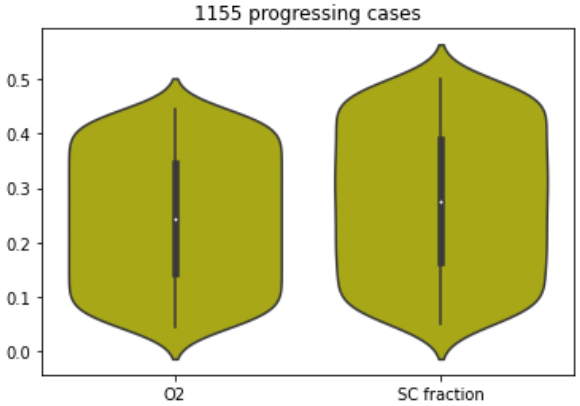

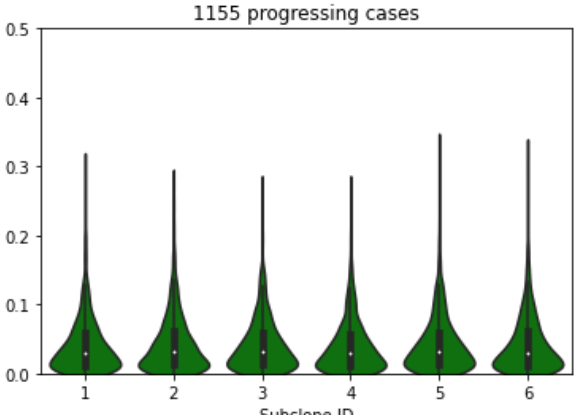

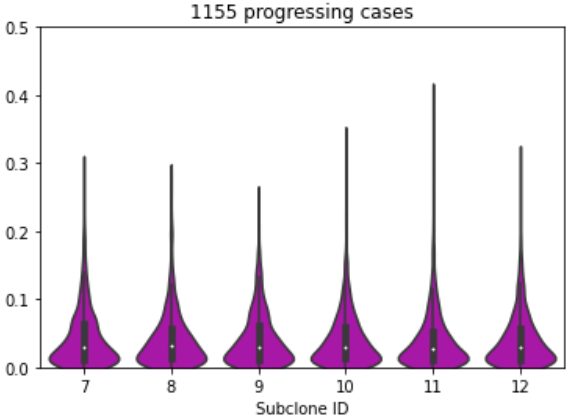

1155 progressing cases.

Input space.
1. Abundant oxygen (left).
2. Uniform initial clone sizes (right).

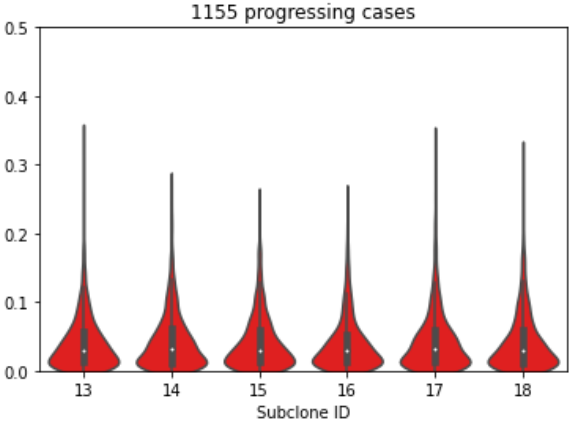

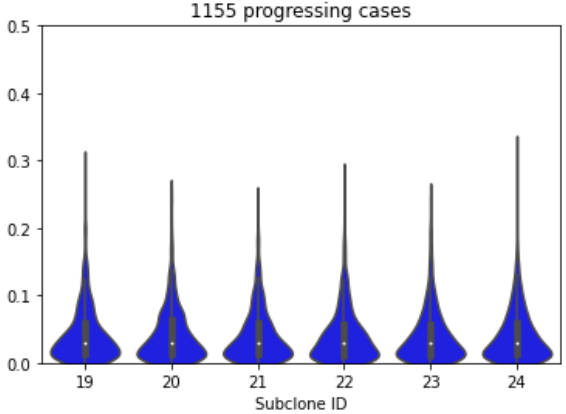

Clonal competition

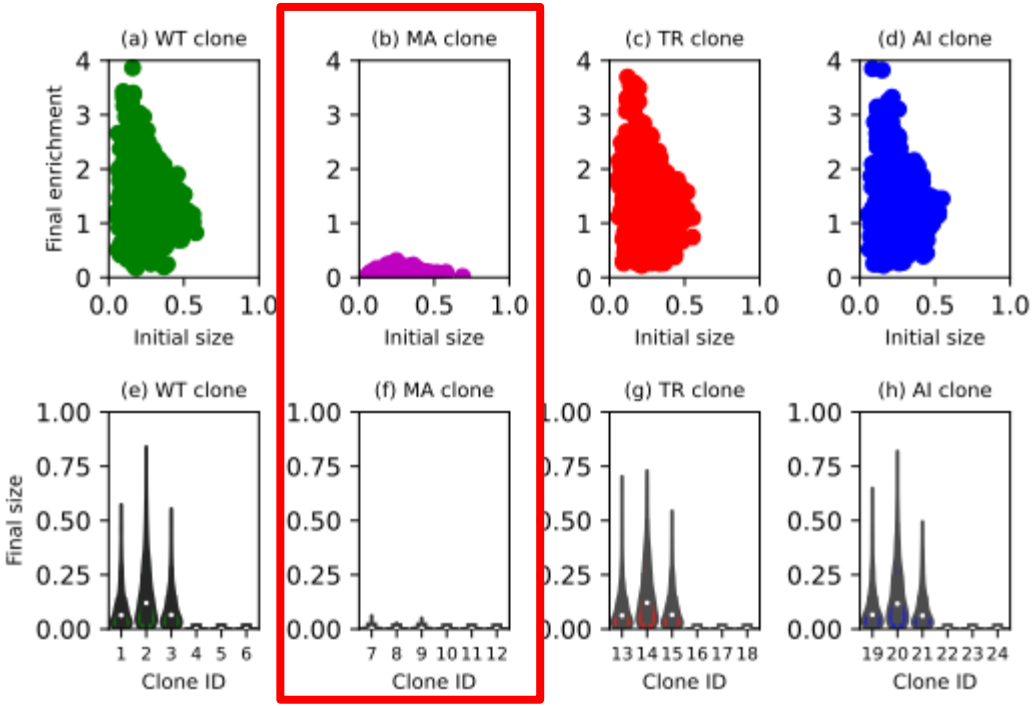

MYCN-amplified clone died!

MA versus WT: p-value < 0.1 %.
1. Student's t-test.
2. Permutation test.

The other three expanded similarly.

ANOVA: p-value > 25 %.
1. F-test.
2. Permutation test.

1155 progressing cases.
Output space: final clone sizes.

Clonal competition

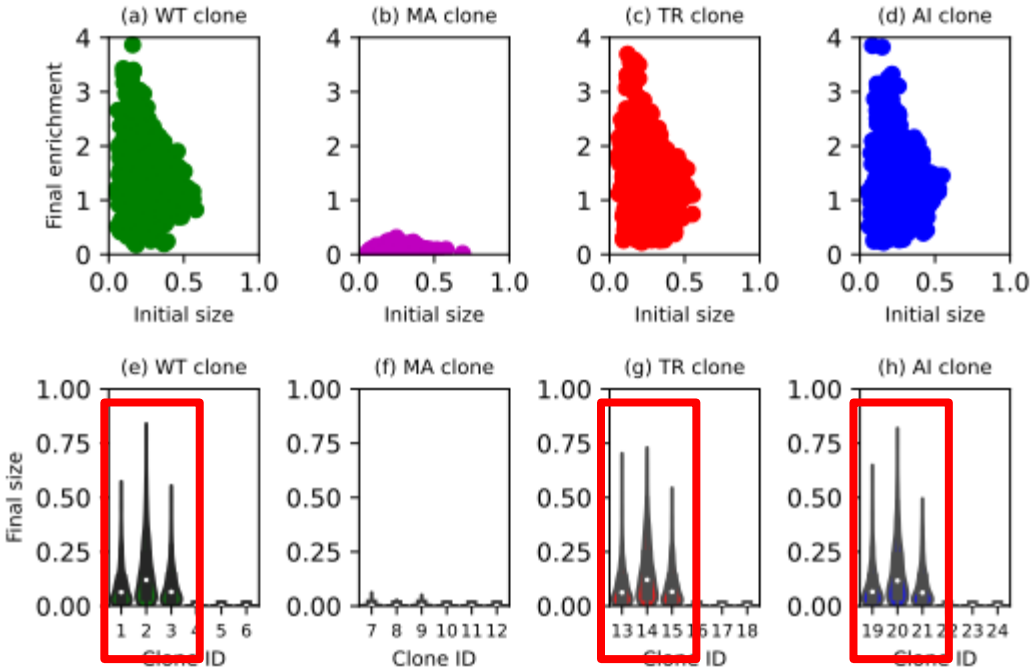

1155 progressing cases.
Output space: final clone sizes.

MYCN-amplified clone died!

MA versus WT: p-value < 0.1 %.
1. Student's t-test.
2. Permutation test.

The other three expanded similarly.

ANOVA: p-value > 25 %.
1. F-test.
2. Permutation test.

The nine growing subclones all had their p53 intact!

Multicellular model

1. Model structure.
2. Model calibration.
3. Clonal competition.
4. **p53 and p73.**
5. Targeted therapies.
6. Surrogate modelling.

p53 and p73

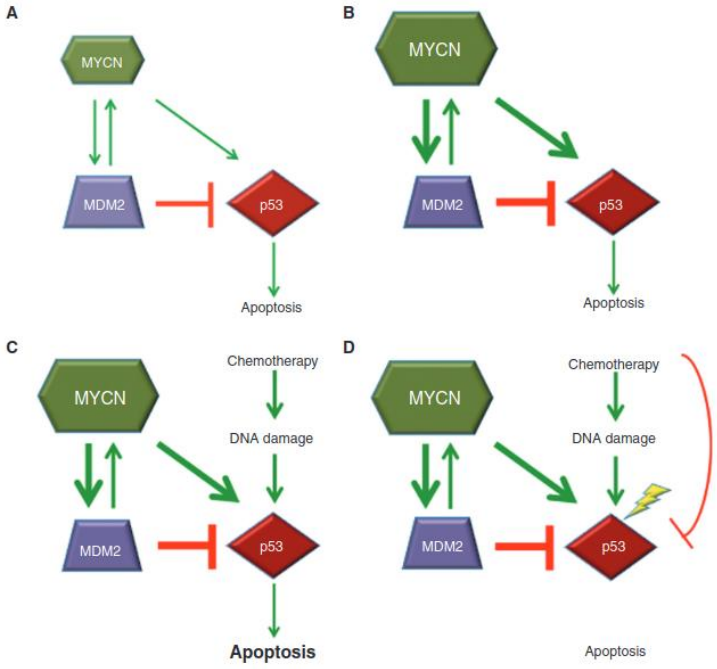

Huang, Miller, and William A. Weiss. "Neuroblastoma and MYCN." *Cold Spring Harbor perspectives in medicine* 3.10 (2013): a014415.

MYCN amplification is associated with p53 inactivation. **This property is in the model.**

Gamble, Laura D., et al. "MYCN sensitizes neuroblastoma to the MDM2-p53 antagonists Nutlin-3 and MI-63." *Oncogene* 31.6 (2012): 752-763.

p53 can trigger **contradictory** cellular functions.
1. Cell cycle arrest.
2. DNA repair.
3. Apoptosis.

p53 has a **context-dependent** and non-linear relationship with the disease outcome.

Context: mechanisms described in the model and the parameters quantifying them.

p53 and p73

Tested the MYCN-amplified clone's sensitivity to the five most important genes.

1000 combinations of gene expression levels.

283 cases where the MYCN-amplified clone expanded drastically.

p53 and p73

MAPK/RAS signalling is described by two parameters.
One was set to be higher.

Tested the MYCN-amplified clone's sensitivity to the five most important genes.

1000 combinations of gene expression levels.

283 cases where the MYCN-amplified clone expanded drastically.

p53 and p73

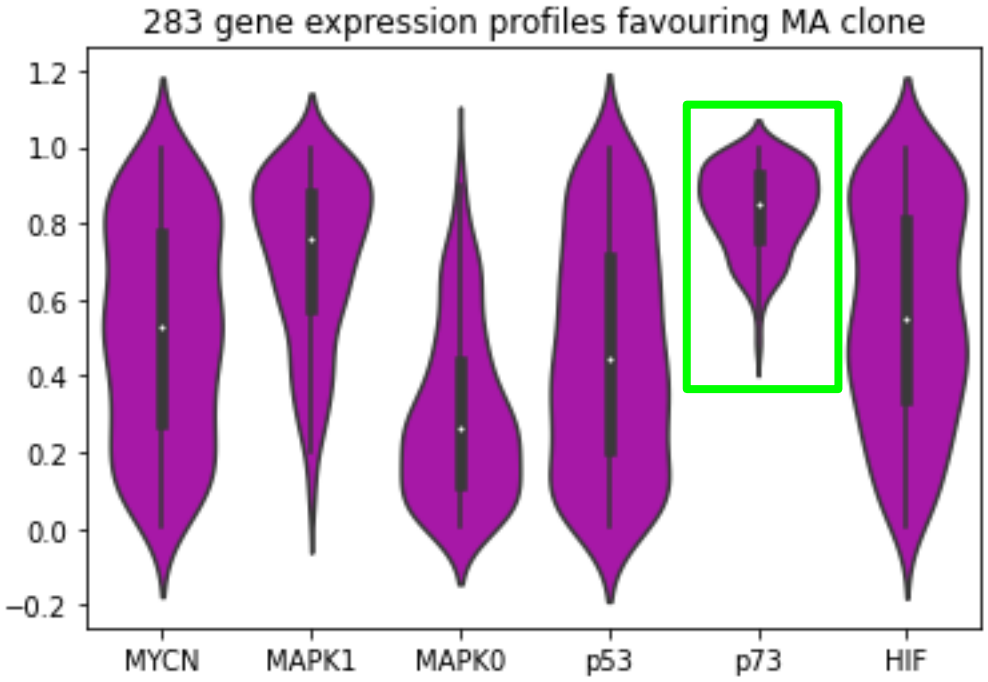

Tested the MYCN-amplified clone's sensitivity to the five most important genes.

1000 combinations of gene expression levels.

283 cases where the MYCN-amplified clone expanded drastically.

p73 can compensate for the loss of p53.

In this context, p53 and p73 promote cell survival more than apoptosis.

Multicellular model

1. Model structure.
2. Model calibration.
3. Clonal competition.
4. p53 and p73.
5. **Targeted therapies.**
6. Surrogate modelling.

Targeted therapies

Step 1. Created a virtual tumour with one large MYCN-amplified clone only.

Step 2. Chose gene expression levels favouring the MYCN-amplified clone.

Step 3. Tested 1000 combinations of drugs targeting the 20 gene products.

20 gene products.Telomerase, ALT, MYCN, MAPK/RAS pathway, JAB1, CHK1, CDS1, CDC25C, ID2, IAP2, HIF, BNIP3, VEGF, p53, p73, p21, p27, Bcl-2/Bcl-xL, BAK/BAX, and CAS.

Targeted therapies

Step 1. Created a virtual tumour with one large MYCN-amplified clone only.

Step 2. Chose gene expression levels favouring the MYCN-amplified clone.

Step 3. Tested 1000 combinations of drugs targeting the 20 gene products.

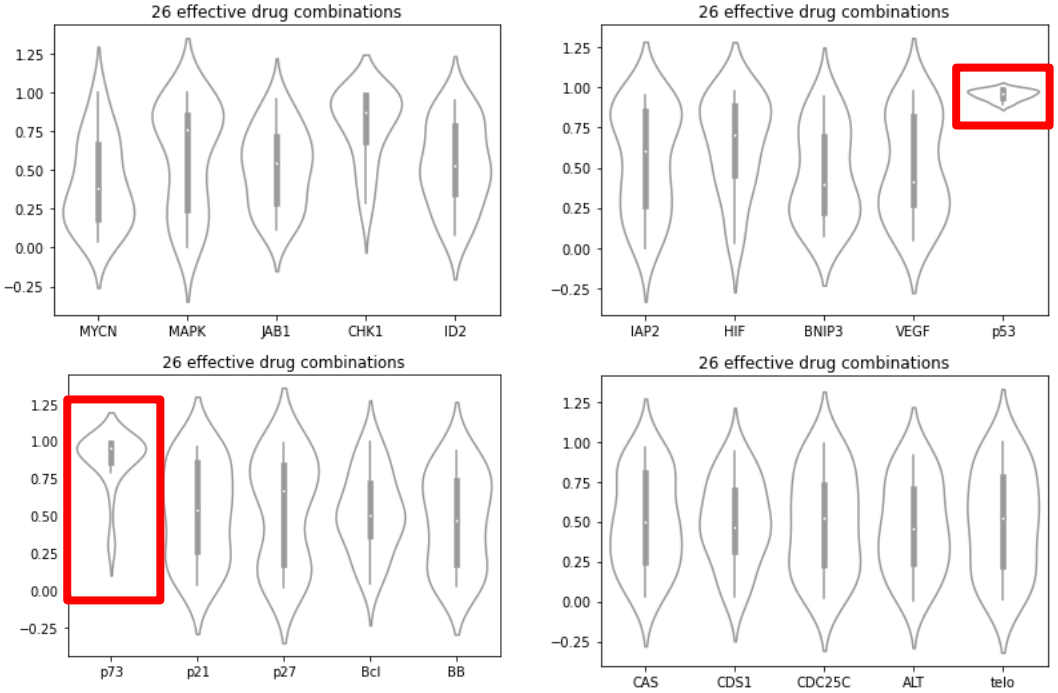

26 drug combinations led to regression.

Inhibiting p53 and p73 is a winning (shrinking) combination.

20 gene products.Telomerase, ALT, MYCN, MAPK/RAS pathway, JAB1, CHK1, CDS1, CDC25C, ID2, IAP2, HIF, BNIP3, VEGF, p53, p73, p21, p27, Bcl-2/Bcl-xL, BAK/BAX, and CAS.

Targeted therapies

Step 1. Created a virtual tumour with one large MYCN-amplified clone only.

Step 2. Chose gene expression levels favouring the MYCN-amplified clone.

Step 3. Tested 1000 combinations of drugs targeting the 20 gene products.

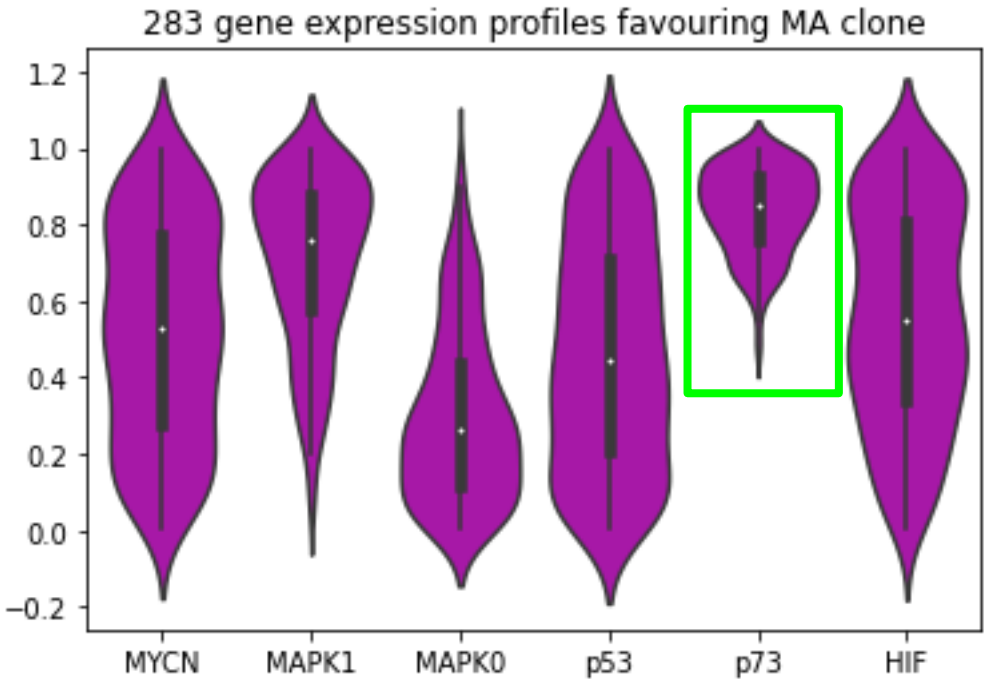

283 gene expression profiles led to expansion.

Although inhibiting p53 only is not.

20 gene products.Telomerase, ALT, MYCN, MAPK/RAS pathway, JAB1, CHK1, CDS1, CDC25C, ID2, IAP2, HIF, BNIP3, VEGF, p53, p73, p21, p27, Bcl-2/Bcl-xL, BAK/BAX, and CAS.

Targeted therapies

Step 1. Created a virtual tumour with one large MYCN-amplified clone only.

Step 2. Chose gene expression levels favouring the MYCN-amplified clone.

Step 3. Tested 1000 combinations of drugs targeting the 20 gene products.

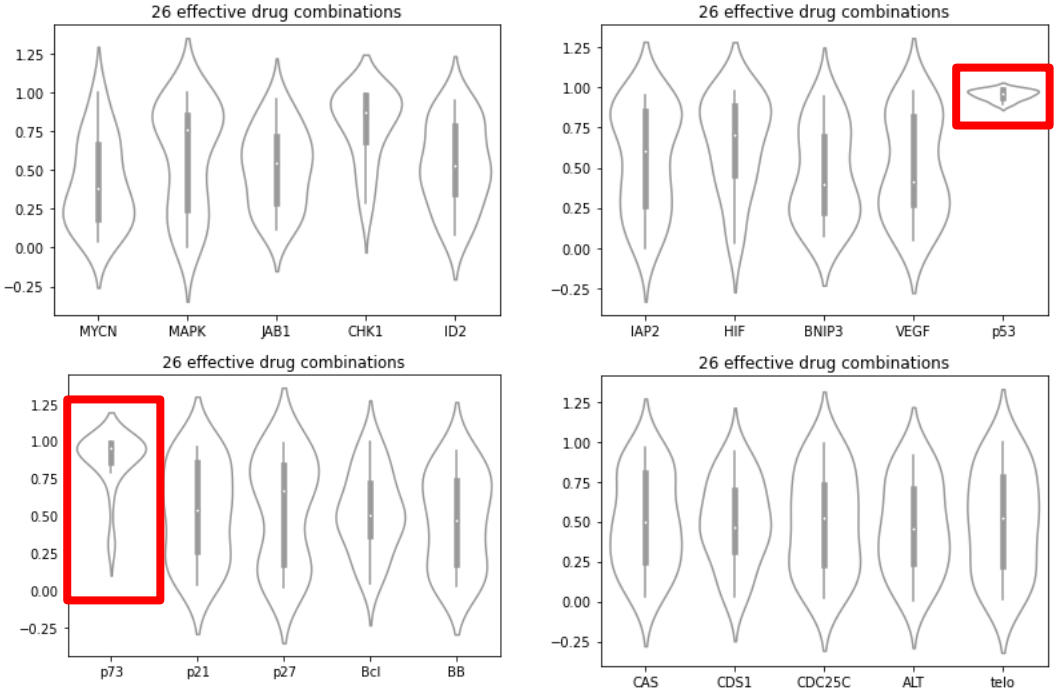

26 drug combinations led to regression.

Inhibiting p53 and p73 is a winning (shrinking) combination.

20 gene products.Telomerase, ALT, MYCN, MAPK/RAS pathway, JAB1, CHK1, CDS1, CDC25C, ID2, IAP2, HIF, BNIP3, VEGF, p53, p73, p21, p27, Bcl-2/Bcl-xL, BAK/BAX, and CAS.

Targeted therapies

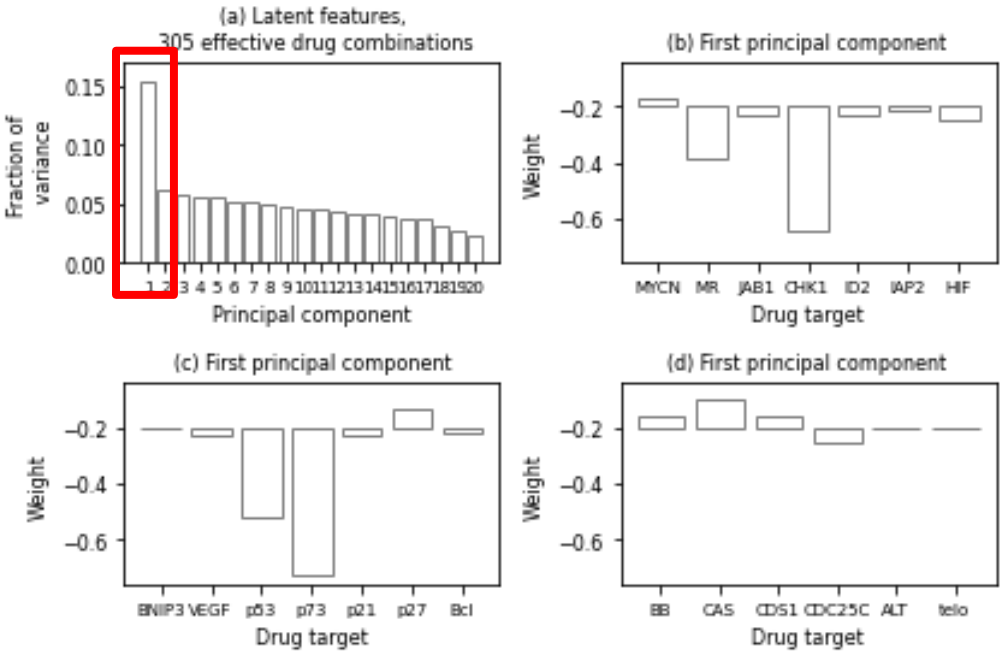

305 most and 297 least effective drug combinations.

Principal component analysis to identify a latent feature in the 20-dimensional input space.

Targeted therapies

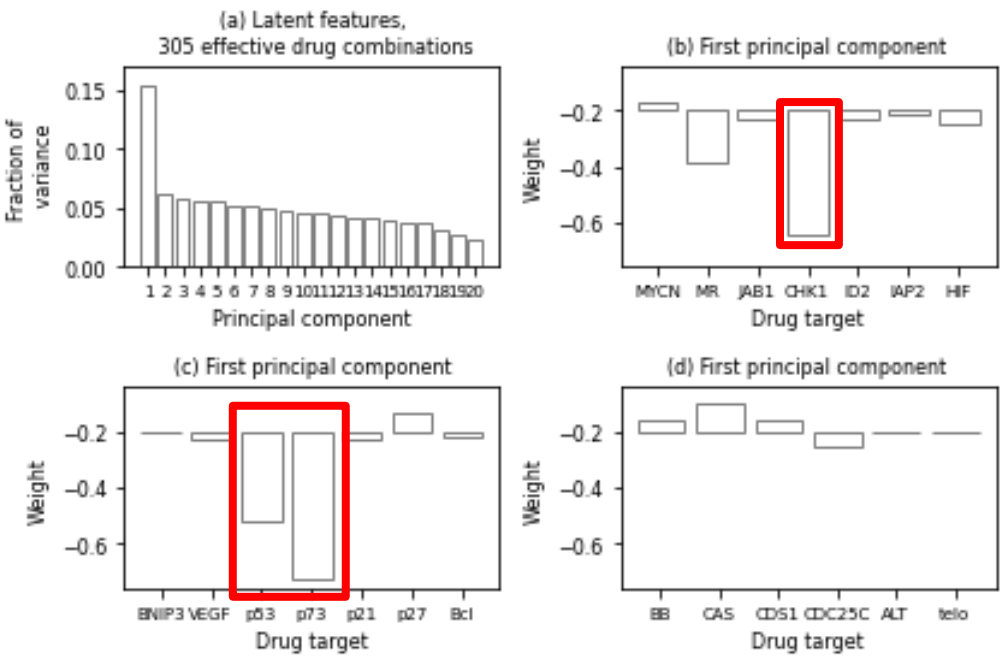

305 most and 297 least effective drug combinations.

Principal component analysis to identify a **latent feature** in the 20-dimensional input space.

Inhibiting CHK1, p53, and p73 is a winning (shrinking) combination.

Note that CHK1 activates p73 in this model.

Targeted therapies

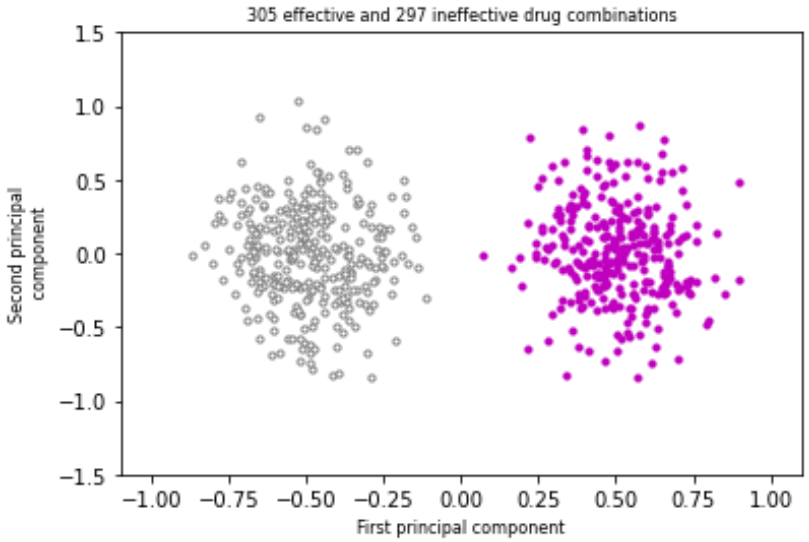

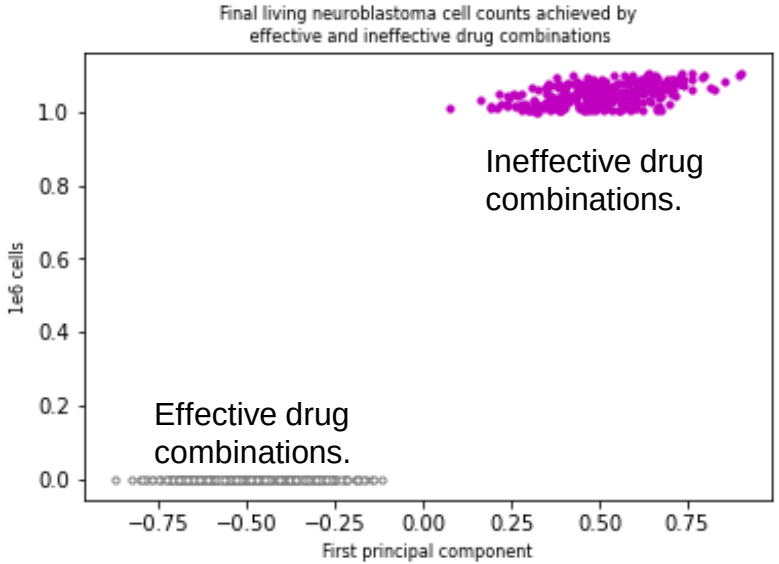

Data projected onto and clustered along the first principal component (PC1).

Plotted along the first two principal components: PC1 and PC2.

The two predicted clusters separate the effective and ineffective drug combinations perfectly.

Silhouette Coefficient > 0.82.

Multicellular model

1. Model structure.
2. Model calibration.
3. Clonal competition.
4. p53 and p73.
5. Targeted therapies.
6. **Surrogate modelling.**

Surrogate modelling

It took around 10 days to evaluate 5000 drug combinations on the most advanced GPUs.

Surrogate modelling

It took around 10 days to evaluate 5000 drug combinations on the most advanced GPUs.

A model of the multicellular model using supervised machine learning methods.

Surrogate modelling

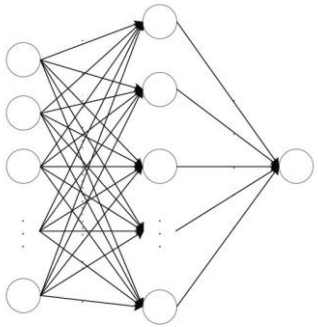

Multilayer perceptron.

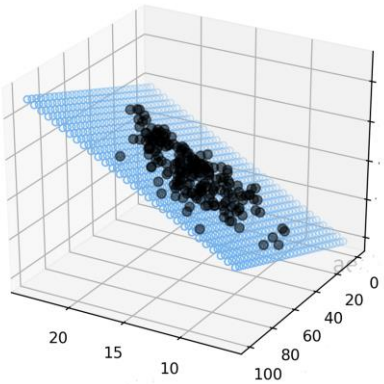

Multiple linear regression.

Surrogate modelling

One drug combination comprises the inhibitory effects on 20 gene products.

20 inputs or features.

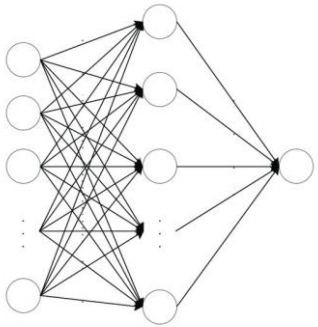

Multilayer perceptron.

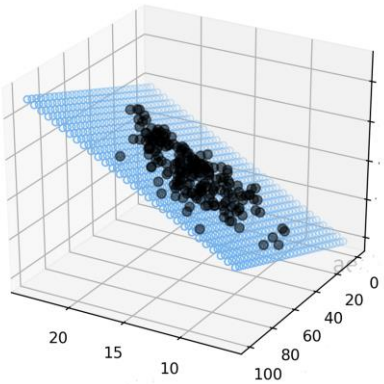

Multiple linear regression.

Surrogate modelling

One drug combination comprises the inhibitory effects on 20 gene products.

20 inputs or features.

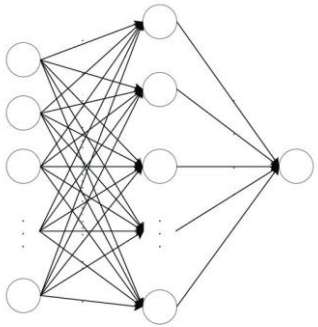

Multilayer perceptron.

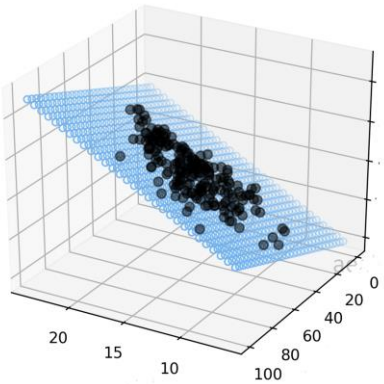

Multiple linear regression.

Final living neuroblastoma cell count.

One output only.

Coefficient of determination > 0.91.

Population model

1. **Induction chemotherapy.**
2. Model structure.
3. Model calibration.
4. Optimisation.

Induction chemotherapy

Current standard:
multi-modal therapy.

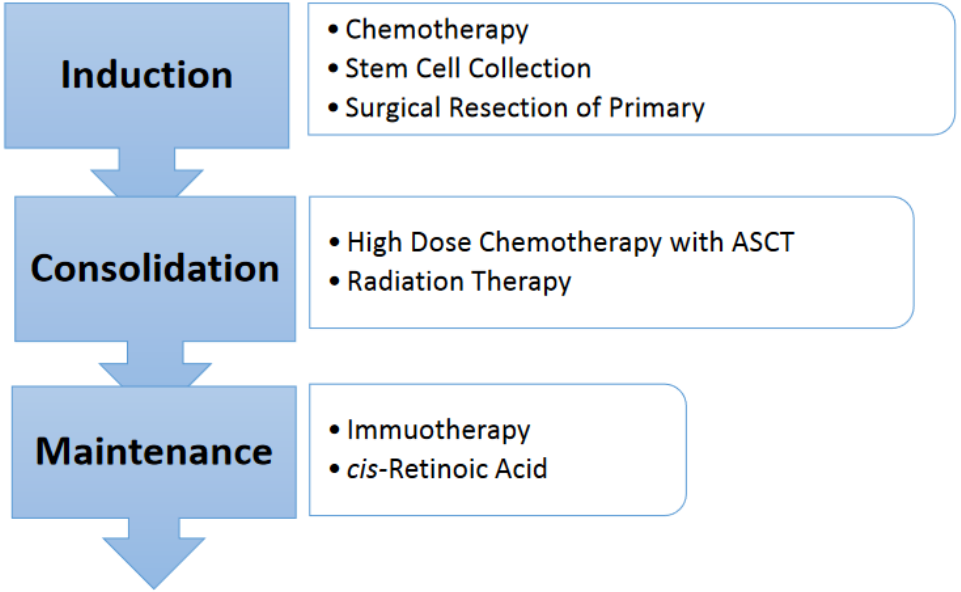

Smith, Valeria, and Jennifer Foster. "High-risk neuroblastoma treatment review." *Children* 5.9 (2018): 114.

Induction chemotherapy

Current standard:
multi-modal therapy.

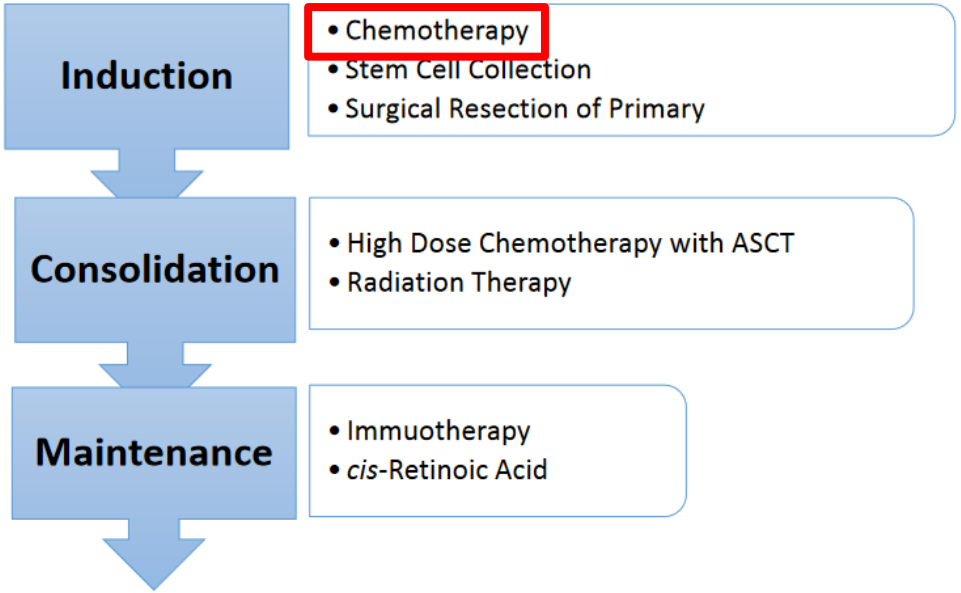

COJEC protocol:

C: cisplatin.
O: vincristine.
J: carboplatin.
E: etoposide.
C: cyclophosphamide.

Smith, Valeria, and Jennifer Foster. "High-risk neuroblastoma treatment review." *Children* 5.9 (2018): 114.

Induction chemotherapy

Current standard:
multi-modal therapy.

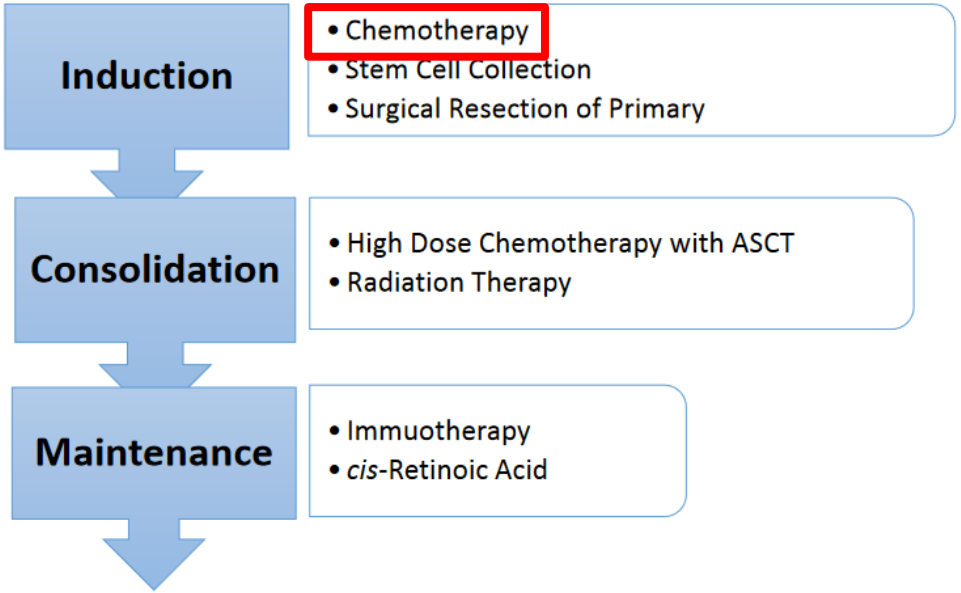

COJEC protocol:

C: cisplatin.
O: vincristine.
J: carboplatin.
E: etoposide.
C: cyclophosphamide.

Eight two-week cycles.

- Alternating combinations.
- Maximum tolerated doses.

One protocol for every patient.

Smith, Valeria, and Jennifer Foster. "High-risk neuroblastoma treatment review." *Children* 5.9 (2018): 114.

Induction chemotherapy

Current standard:
multi-modal therapy.

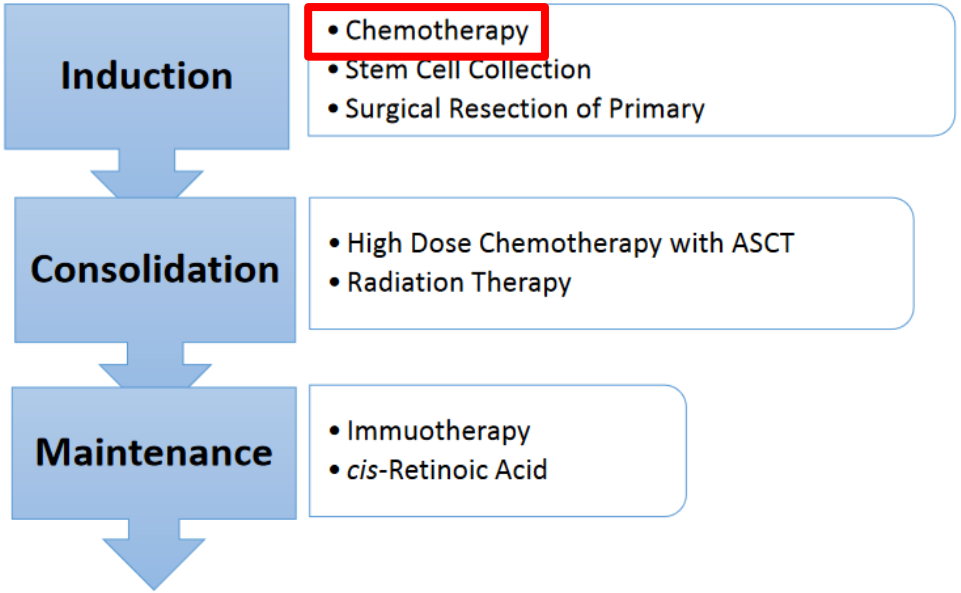

COJEC protocol:

C: cisplatin.
O: vincristine.
J: carboplatin.
E: etoposide.
C: cyclophosphamide.

Optimise a two-drug protocol with respect to the tumour's initial composition.

- Number of cycles.
- Doses in each cycle.

Smith, Valeria, and Jennifer Foster. "High-risk neuroblastoma treatment review." *Children* 5.9 (2018): 114.

Population model

1. Induction chemotherapy.
2. **Model structure.**
3. Model calibration.
4. Optimisation.

Model structure

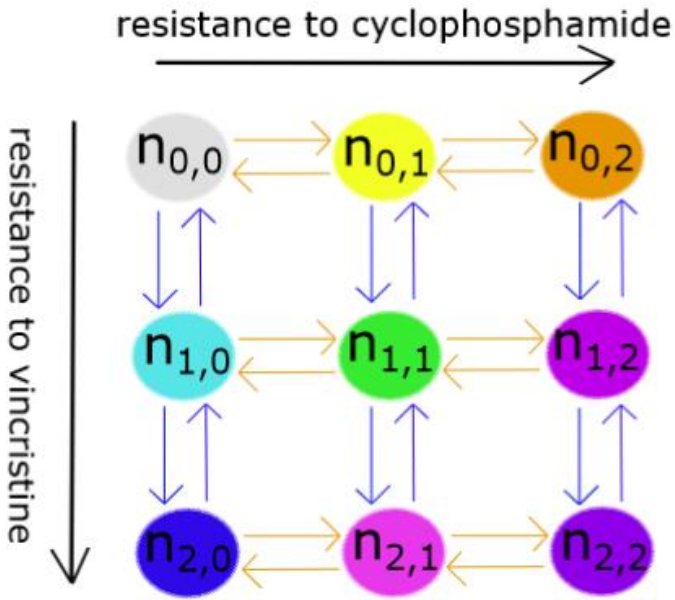

Model structure

$$\frac{dn_{i,j}(t)}{dt} = \frac{G(t)}{1+\alpha_r\phi(\tau)} - \frac{M(t)}{1+\alpha_r\phi(\tau)} - \frac{D(t)}{1+\alpha_m\phi(\tau)}$$

One ordinary differential equation for each clone.

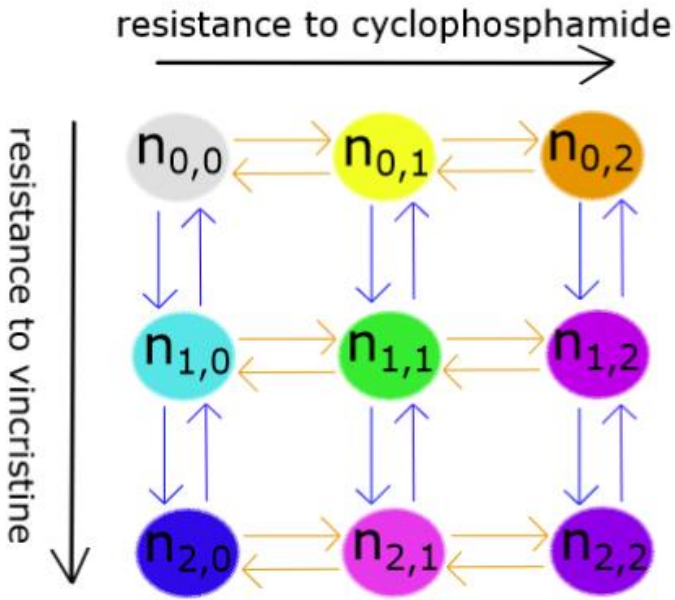

Model structure

$$\frac{dn_{i,j}(t)}{dt} = \boxed{\frac{G(t)}{1+\alpha_r\phi(\tau)}} - \frac{M(t)}{1+\alpha_r\phi(\tau)} - \frac{D(t)}{1+\alpha_m\phi(\tau)}$$

One ordinary differential equation for each clone.

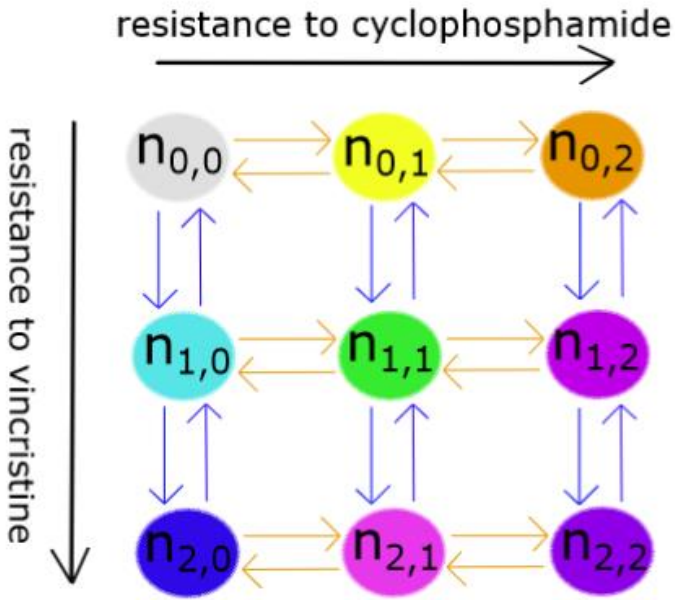

$G(t) = \left(1 - \frac{\sum_{k,l} n_{k,l}(t)}{K}\right)\left(r_{i,j} n_{i,j}(t)\right)$ is the logistic **growth rate**

Model structure

$$\frac{dn_{i,j}(t)}{dt} = \frac{G(t)}{1+\alpha_r\phi(\tau)} - \boxed{\frac{M(t)}{1+\alpha_r\phi(\tau)}} - \frac{D(t)}{1+\alpha_m\phi(\tau)}$$

One ordinary differential equation for each clone.

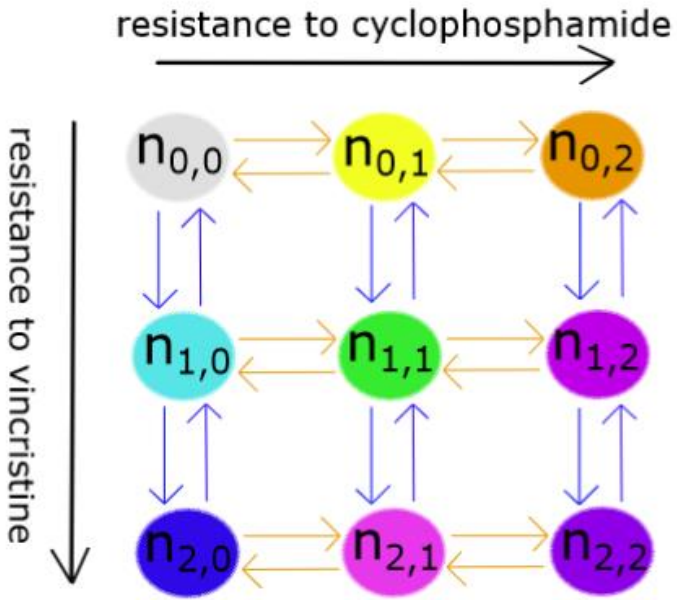

$G(t) = \left(1 - \frac{\sum_{k,l} n_{k,l}(t)}{K}\right)\left(r_{i,j} n_{i,j}(t)\right)$ is the logistic **growth rate**

$M(t) = \mu\left(1 - \frac{\sum_{k,l} n_{k,l}(t)}{K}\right)\left(\gamma_{i,j} r_{i,j} n_{i,j}(t) - \sum_{p,q} r_{p,q} n_{p,q}(t)\right)$

is the result of **mutation** events

Model structure

$$\frac{dn_{i,j}(t)}{dt} = \frac{G(t)}{1+\alpha_r\phi(\tau)} - \frac{M(t)}{1+\alpha_r\phi(\tau)} - \boxed{\frac{D(t)}{1+\alpha_m\phi(\tau)}}$$

One ordinary differential equation for each clone.

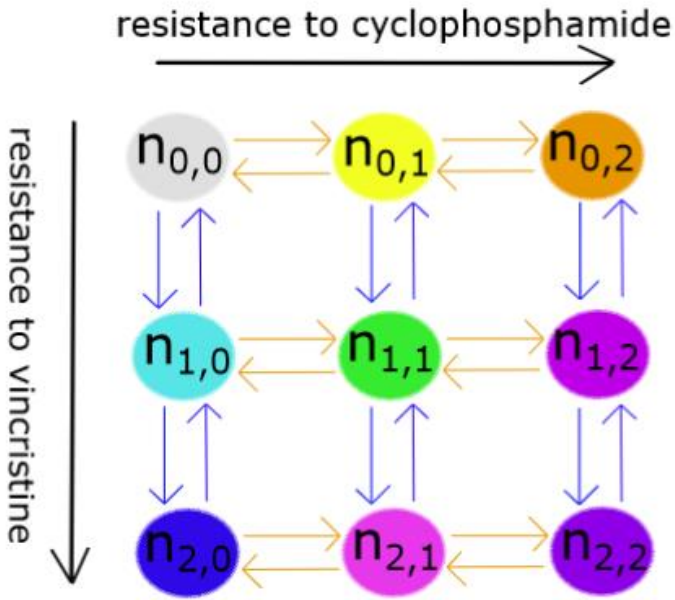

$G(t) = \left(1 - \frac{\sum_{k,l} n_{k,l}(t)}{K}\right)\left(r_{i,j} n_{i,j}(t)\right)$ is the logistic **growth rate**

$M(t) = \mu\left(1 - \frac{\sum_{k,l} n_{k,l}(t)}{K}\right)\left(\gamma_{i,j} r_{i,j} n_{i,j}(t) - \sum_{p,q} r_{p,q} n_{p,q}(t)\right)$

is the result of **mutation** events

$D(t) = \sum_d m_d^{i,j}(c_d(t)) n_{i,j}(t)$ is the rate of **drug-induced death**

Model structure

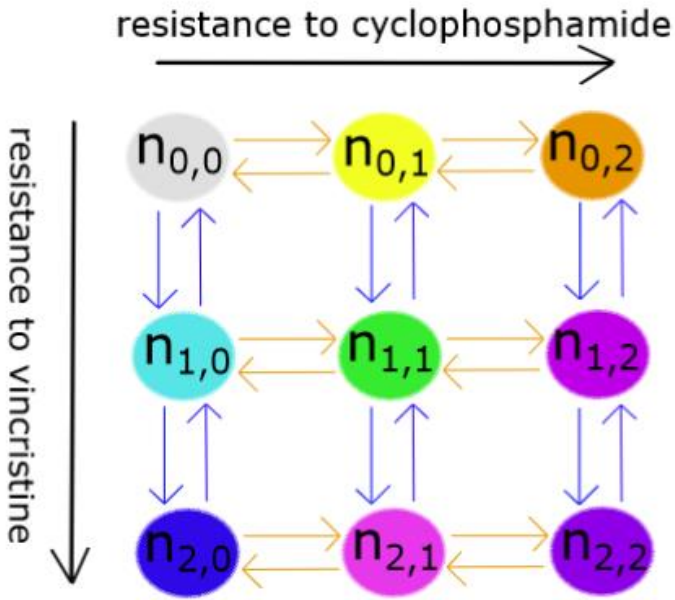

$$\frac{dn_{i,j}(t)}{dt} = \frac{G(t)}{1+\alpha_r\phi(\tau)} - \frac{M(t)}{1+\alpha_r\phi(\tau)} - \frac{D(t)}{1+\alpha_m\phi(\tau)}$$

One ordinary differential equation for each clone.

$G(t) = \left(1 - \frac{\sum_{k,l} n_{k,l}(t)}{K}\right)\left(r_{i,j}n_{i,j}(t)\right)$ is the logistic **growth rate**

$M(t) = \mu\left(1 - \frac{\sum_{k,l} n_{k,l}(t)}{K}\right)\left(\gamma_{i,j}r_{i,j}n_{i,j}(t) - \sum_{p,q} r_{p,q}n_{p,q}(t)\right)$

is the result of **mutation** events

$D(t) = \sum_d m_d^{i,j}(c_d(t))n_{i,j}(t)$ is the rate of **drug-induced death**

$$\frac{dc_d(t)}{dt} = \omega_d(t) - z_d c_d(t), \quad d = 1, 2$$

Two first-order pharmacokinetic equations for vincristine and cyclophosphamide.

Population model

1. Induction chemotherapy.
2. Model structure.
3. **Model calibration.**
4. Optimisation.

Model calibration

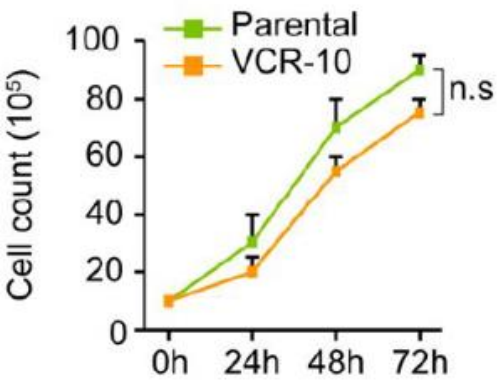

Jemaà, Mohamed, et al. "Gene expression signature of acquired chemoresistance in neuroblastoma cells." *International Journal of Molecular Sciences* 21.18 (2020): 6811.

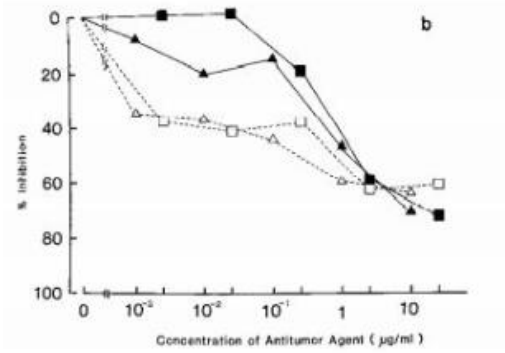

Zaizen, Y., A. Nakagawara, and K. Ikeda. "Patterns of destruction of mouse neuroblastoma cells by extracellular hydrogen peroxide formed by 6-hydroxydopamine and ascorbate." *Journal of cancer research and clinical oncology* 111 (1986): 93-97.

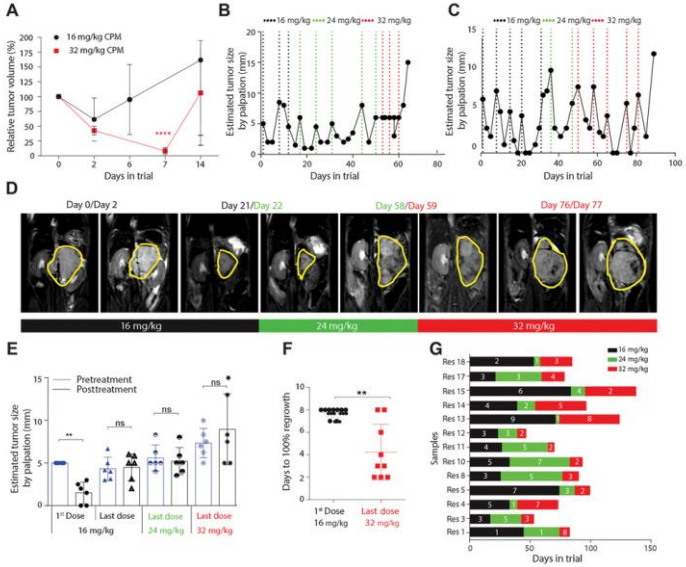

Yogev, Orli, et al. "In Vivo Modeling of Chemoresistant Neuroblastoma Provides New Insights into Chemorefractory Disease and MetastasisModeling Chemoresistance and Metastasis in Neuroblastoma." *Cancer research* 79.20 (2019): 5382-5393.

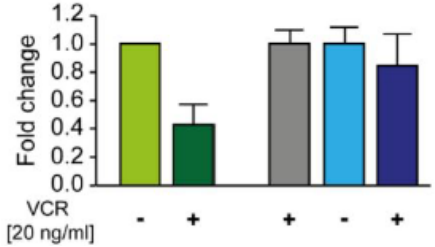

Jemaà, Mohamed, et al. "Gene expression signature of acquired chemoresistance in neuroblastoma cells." *International Journal of Molecular Sciences* 21.18 (2020): 6811.

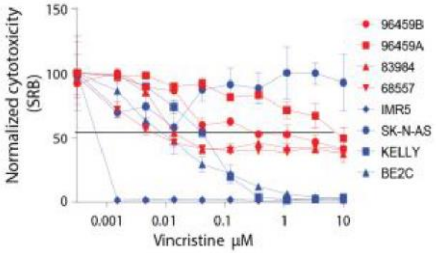

Yogev, Orli, et al. "In Vivo Modeling of Chemoresistant Neuroblastoma Provides New Insights into Chemorefractory Disease and MetastasisModeling Chemoresistance and Metastasis in Neuroblastoma." *Cancer research* 79.20 (2019): 5382-5393.

Model calibration

Levenberg-Marquardt algorithm.

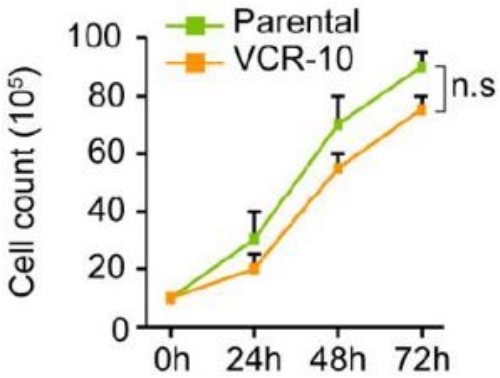

Jemaà, Mohamed, et al. "Gene expression signature of acquired chemoresistance in neuroblastoma cells." *International Journal of Molecular Sciences* 21.18 (2020): 6811.

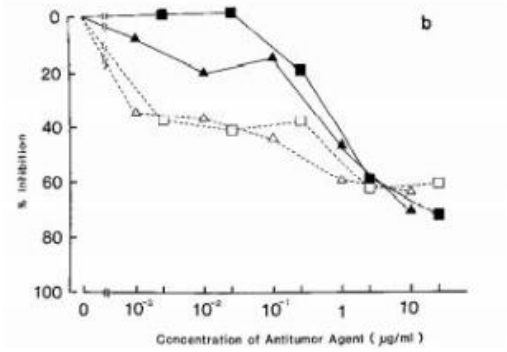

Zaizen, Y., A. Nakagawara, and K. Ikeda. "Patterns of destruction of mouse neuroblastoma cells by extracellular hydrogen peroxide formed by 6-hydroxydopamine and ascorbate." *Journal of cancer research and clinical oncology* 111 (1986): 93-97.

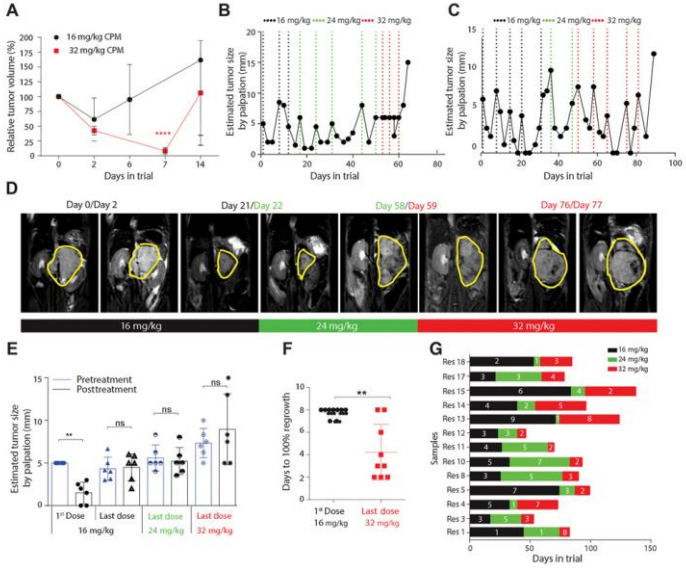

Yogev, Orli, et al. "In Vivo Modeling of Chemoresistant Neuroblastoma Provides New Insights into Chemorefractory Disease and MetastasisModeling Chemoresistance and Metastasis in Neuroblastoma." *Cancer research* 79.20 (2019): 5382-5393.

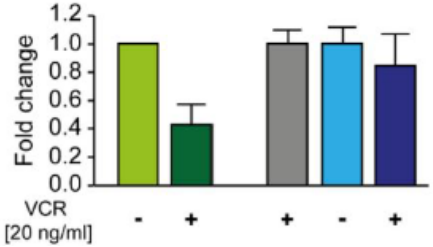

Jemaà, Mohamed, et al. "Gene expression signature of acquired chemoresistance in neuroblastoma cells." *International Journal of Molecular Sciences* 21.18 (2020): 6811.

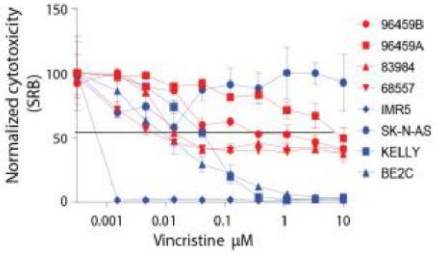

Yogev, Orli, et al. "In Vivo Modeling of Chemoresistant Neuroblastoma Provides New Insights into Chemorefractory Disease and MetastasisModeling Chemoresistance and Metastasis in Neuroblastoma." *Cancer research* 79.20 (2019): 5382-5393.

Model calibration

Levenberg-Marquardt algorithm.
It involves gradient descent.

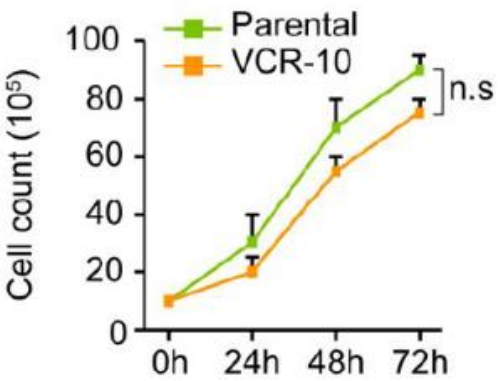

Jemaà, Mohamed, et al. "Gene expression signature of acquired chemoresistance in neuroblastoma cells." *International Journal of Molecular Sciences* 21.18 (2020): 6811.

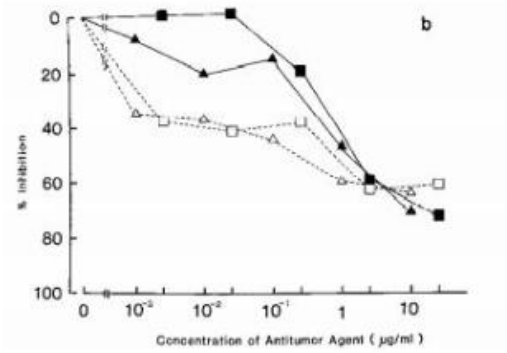

Zaizen, Y., A. Nakagawara, and K. Ikeda. "Patterns of destruction of mouse neuroblastoma cells by extracellular hydrogen peroxide formed by 6-hydroxydopamine and ascorbate." *Journal of cancer research and clinical oncology* 111 (1986): 93-97.

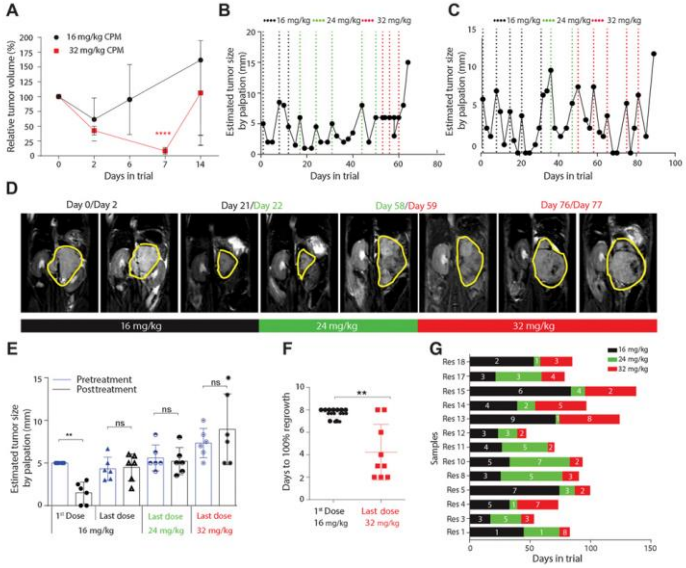

Yogev, Orli, et al. "In Vivo Modeling of Chemoresistant Neuroblastoma Provides New Insights into Chemorefractory Disease and MetastasisModeling Chemoresistance and Metastasis in Neuroblastoma." *Cancer research* 79.20 (2019): 5382-5393.

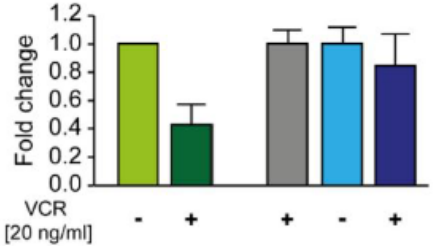

Jemaà, Mohamed, et al. "Gene expression signature of acquired chemoresistance in neuroblastoma cells." *International Journal of Molecular Sciences* 21.18 (2020): 6811.

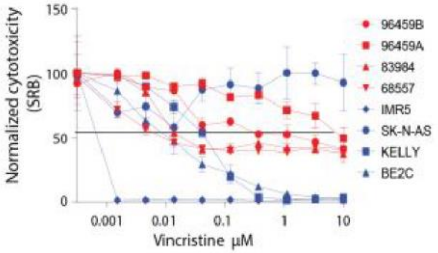

Yogev, Orli, et al. "In Vivo Modeling of Chemoresistant Neuroblastoma Provides New Insights into Chemorefractory Disease and MetastasisModeling Chemoresistance and Metastasis in Neuroblastoma." *Cancer research* 79.20 (2019): 5382-5393.

Population model

1. Induction chemotherapy.
2. Model structure.
3. Model calibration.
4. **Optimisation.**

Optimisation

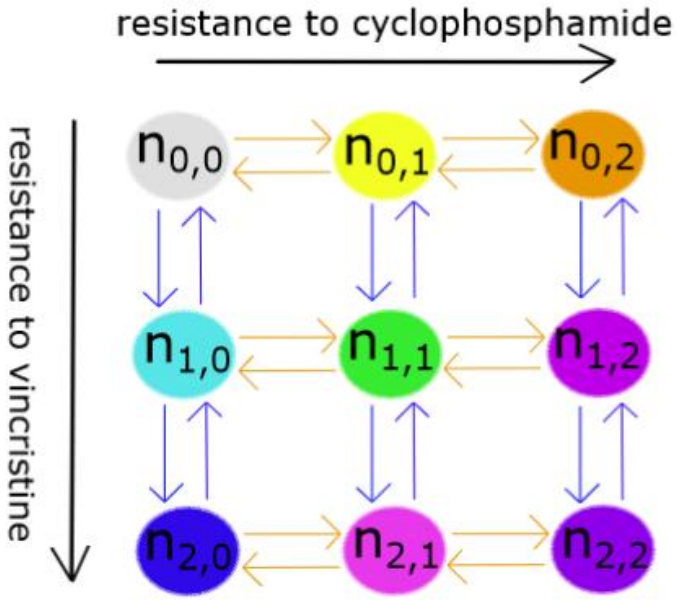

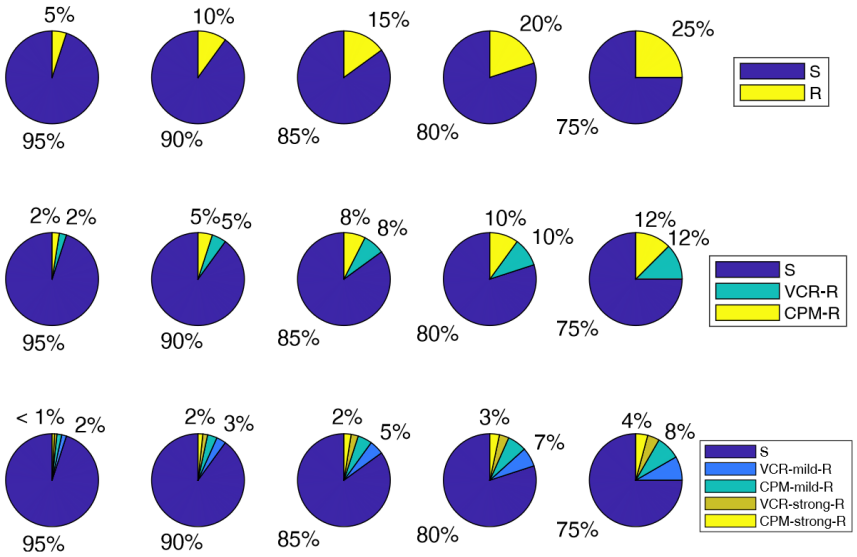

36 initial clonal compositions.

Different distributions of neuroblastoma cells between the nine clones in the model.

Optimisation

Current standard:
multi-modal therapy.

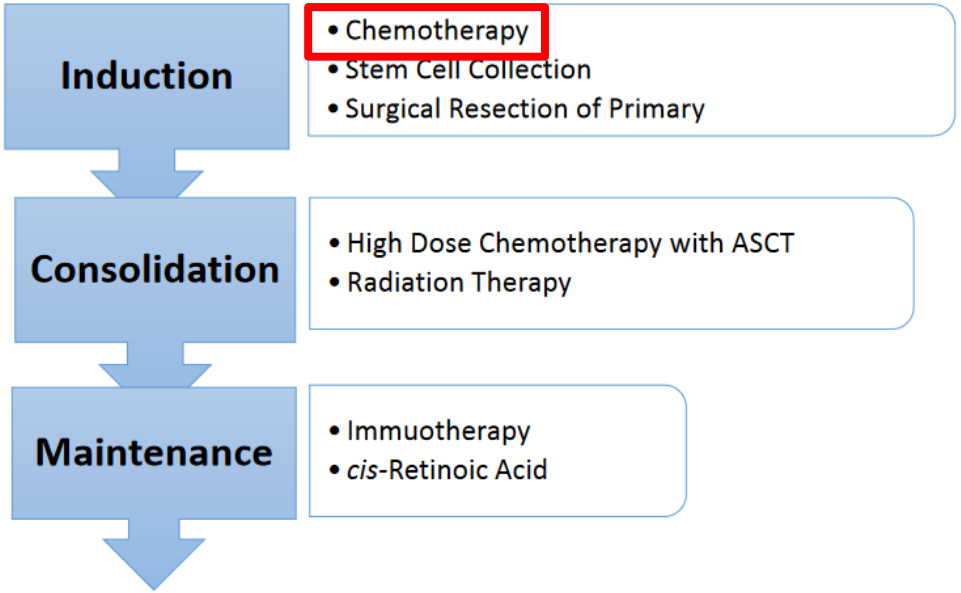

COJEC protocol:

C: cisplatin.
O: vincristine.
J: carboplatin.
E: etoposide.
C: cyclophosphamide.

Optimise a two-drug protocol with respect to the tumour's initial composition.

- Number of cycles.
- Doses in each cycle.

Smith, Valeria, and Jennifer Foster. "High-risk neuroblastoma treatment review." *Children* 5.9 (2018): 114.

Optimisation

Current standard:
multi-modal therapy.

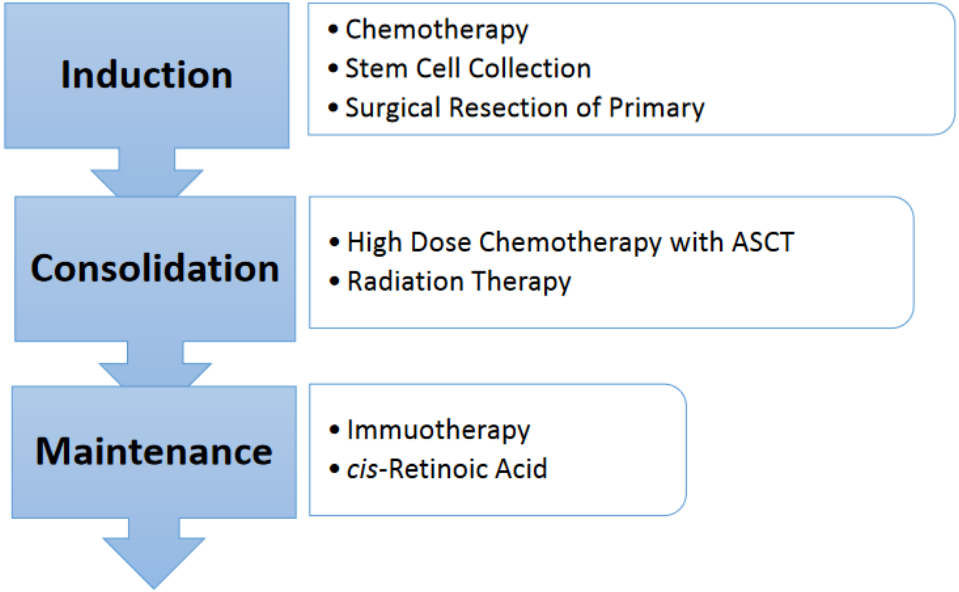

Smith, Valeria, and Jennifer Foster. "High-risk neuroblastoma treatment review." *Children* 5.9 (2018): 114.

COJEC protocol:

C: cisplatin.
O: vincristine.
J: carboplatin.
E: etoposide.
C: cyclophosphamide.

Optimise a two-drug protocol with respect to the tumour's initial composition.

- Number of cycles.
- Doses in each cycle.

Up to 12 cycles, two drugs.
Chemotherapy schedule = 24 doses.

Optimisation

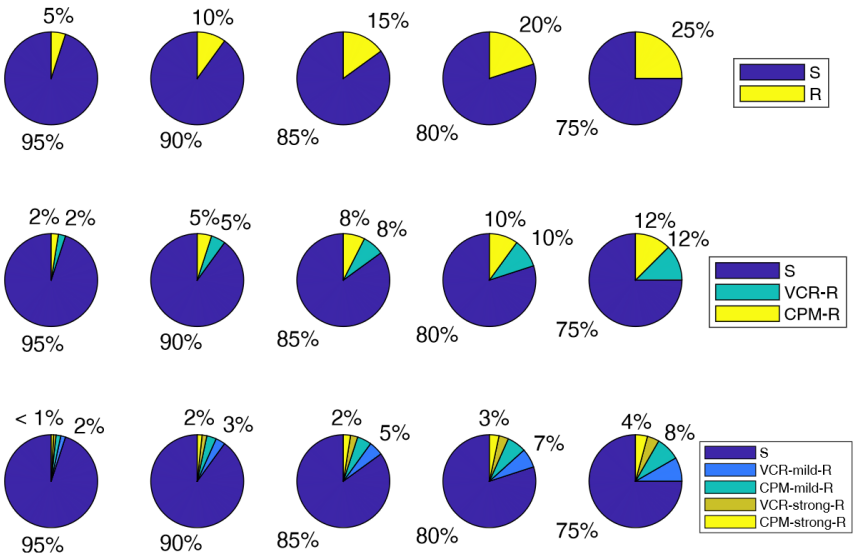

36 initial clonal compositions.

Different distributions of neuroblastoma cells between the nine clones in the model.

Optimisation

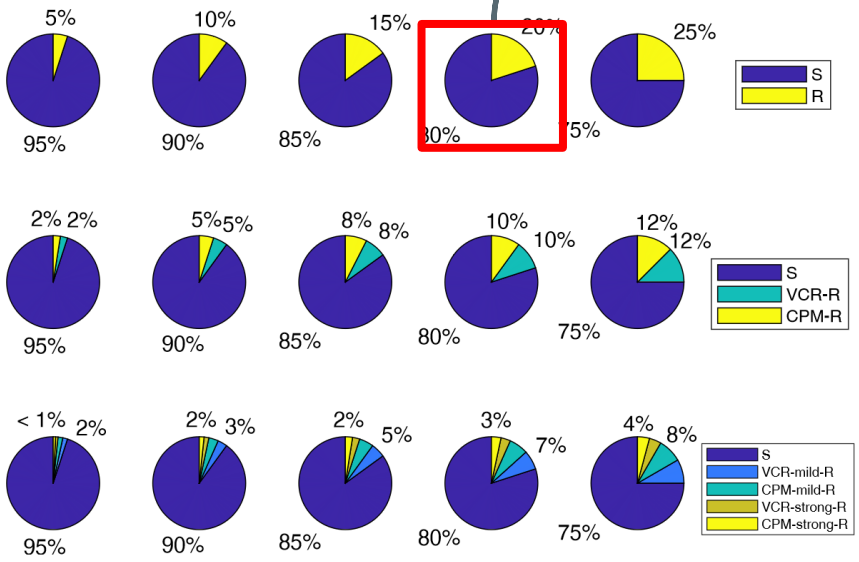

36 initial clonal compositions.

Different distributions of neuroblastoma cells between the nine clones in the model.

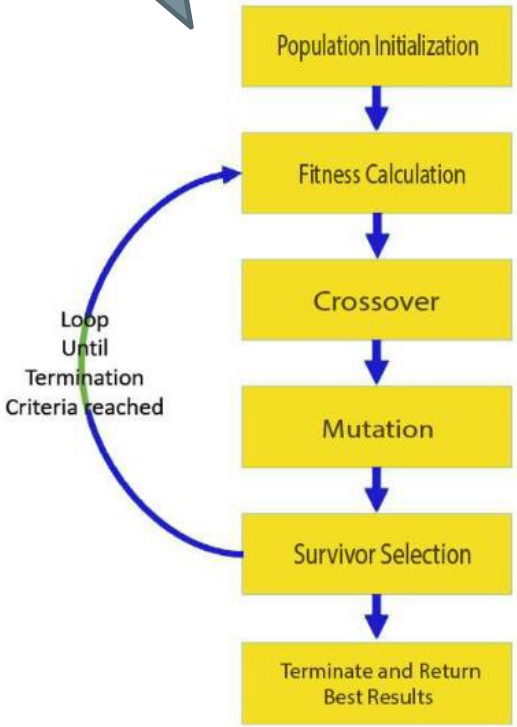

A genetic algorithm mimics the process of natural selection.

Haldurai, Lingaraj, T. Madhubala, and R. Rajalakshmi. "A study on genetic algorithm and its applications." *Int. J. Comput. Sci. Eng* 4.10 (2016): 139-143.

Optimisation

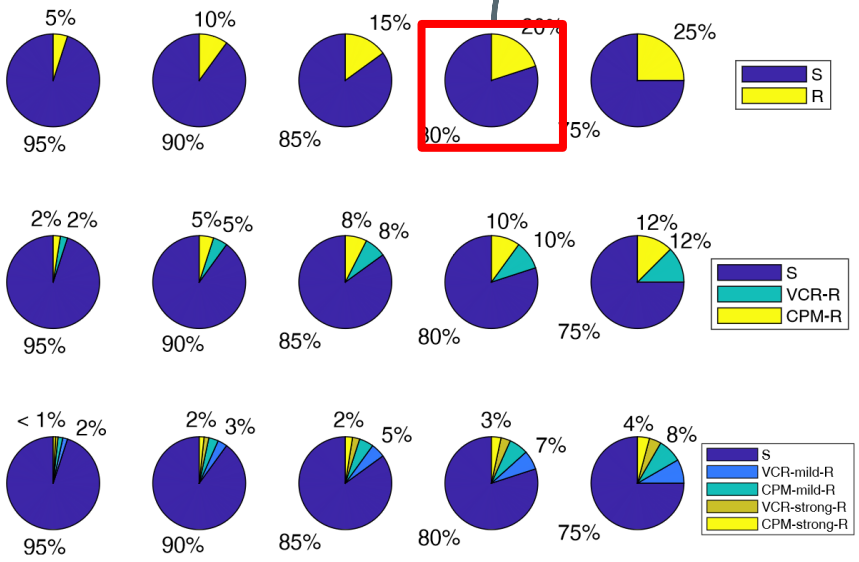

36 initial clonal compositions.

Different distributions of neuroblastoma cells between the nine clones in the model.

One schedule, 24 doses.
One chromosome, 24 genes.

0.1	0.5	1.9	0.2	0.6	0.7	1.1	0.2	1.5	0.4	0.3	1.7	1.1	0.1	0.9	0.6	1.3	0.2	0.3	1.6	0.1	0.7	1.8	0.3

100 random chromosomes.

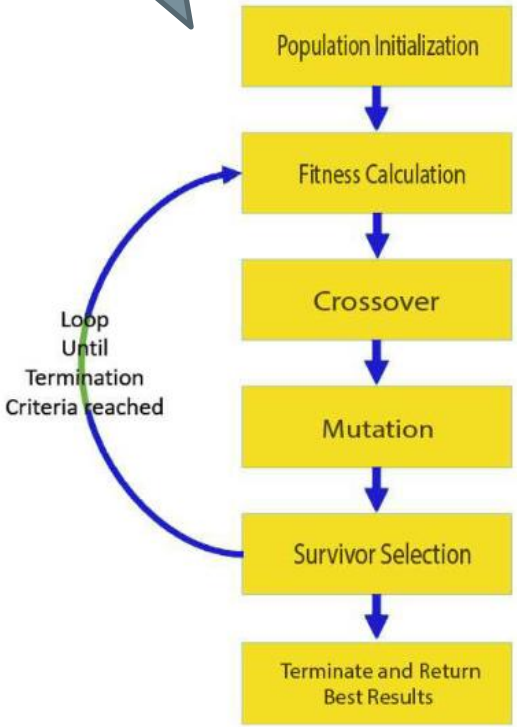

Haldurai, Lingaraj, T. Madhubala, and R. Rajalakshmi. "A study on genetic algorithm and its applications." *Int. J. Comput. Sci. Eng* 4.10 (2016): 139-143.

Optimisation

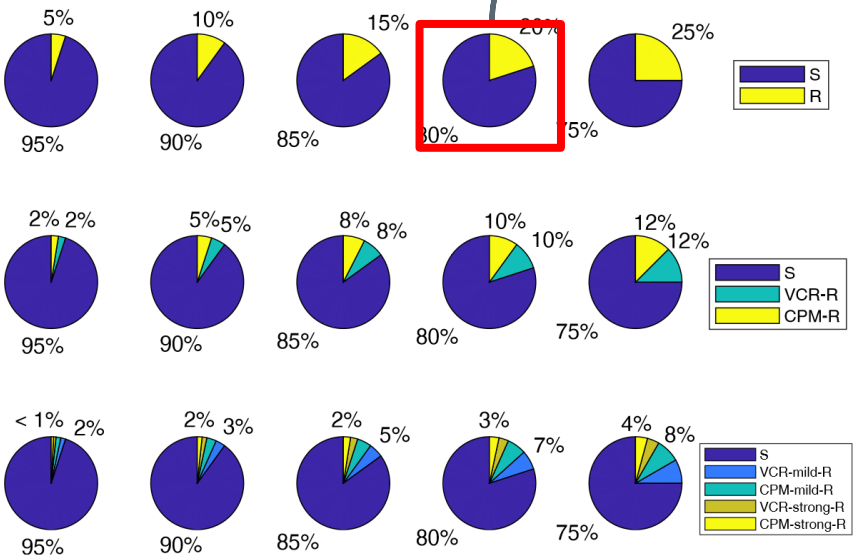

36 initial clonal compositions.

Different distributions of neuroblastoma cells between the nine clones in the model.

One schedule, 24 doses.
One chromosome, 24 genes.

0.1	0.5	1.9	0.2	0.6	0.7	1.1	0.2	1.5	0.4	0.3	1.7	1.1	0.1	0.9	0.6	1.3	0.2	0.3	1.6	0.1	0.7	1.8	0.3

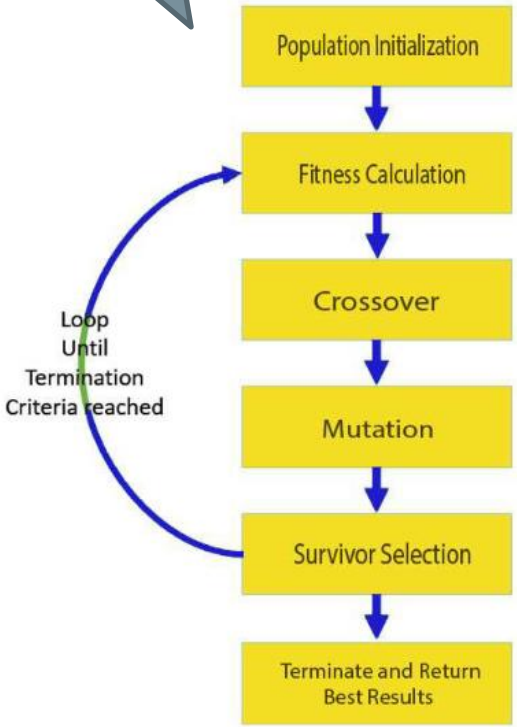

100 random chromosomes.

Ability to shrink the tumour.

Haldurai, Lingaraj, T. Madhubala, and R. Rajalakshmi. "A study on genetic algorithm and its applications." *Int. J. Comput. Sci. Eng* 4.10 (2016): 139-143.

Optimisation

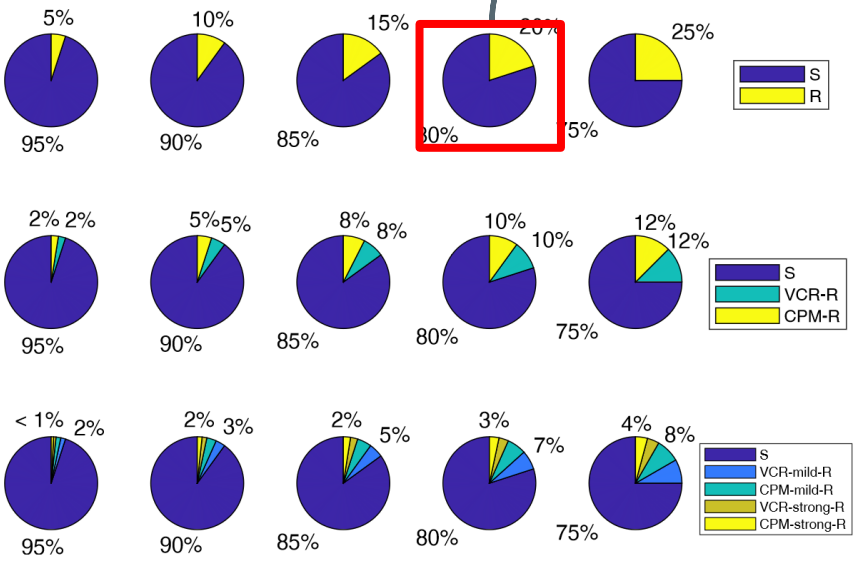

36 initial clonal compositions.

Different distributions of neuroblastoma cells between the nine clones in the model.

One schedule, 24 doses.
One chromosome, 24 genes.

0.1	0.5	1.9	0.2	0.6	0.7	1.1	0.2	1.5	0.4	0.3	1.7	1.1	0.1	0.9	0.6	1.3	0.2	0.3	1.6	0.1	0.7	1.8	0.3

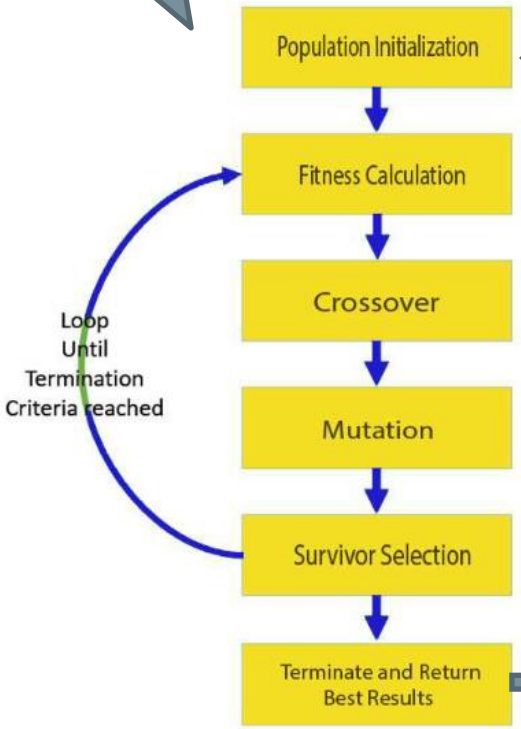

100 random chromosomes.

Ability to shrink the tumour.

Refinement by gradient descent.

Haldurai, Lingaraj, T. Madhubala, and R. Rajalakshmi. "A study on genetic algorithm and its applications." *Int. J. Comput. Sci. Eng* 4.10 (2016): 139-143.

Optimisation

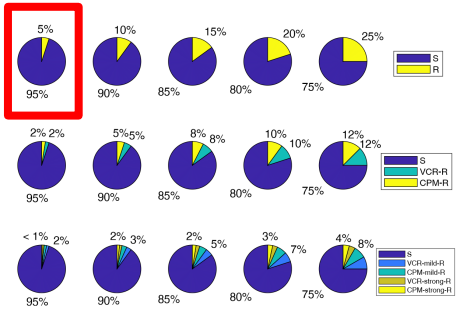

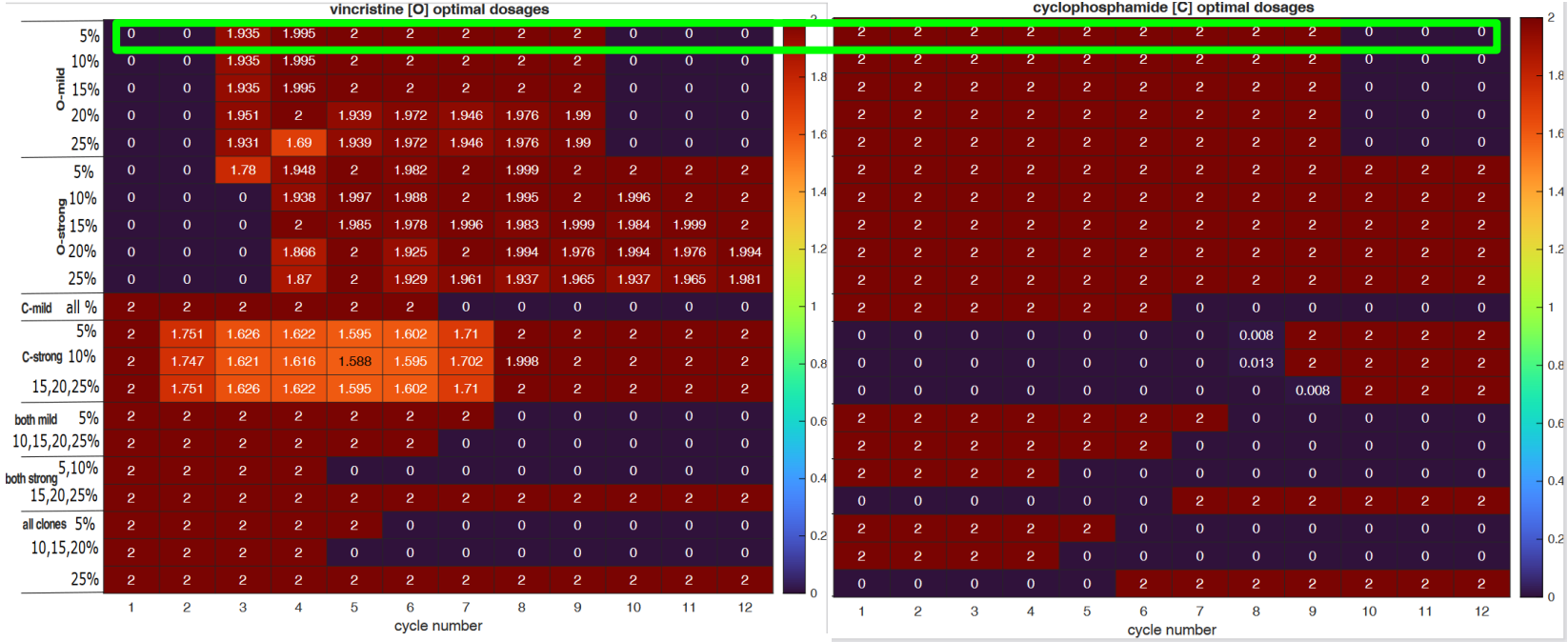

Optimisation

Heat maps are effective tools for visualisation.

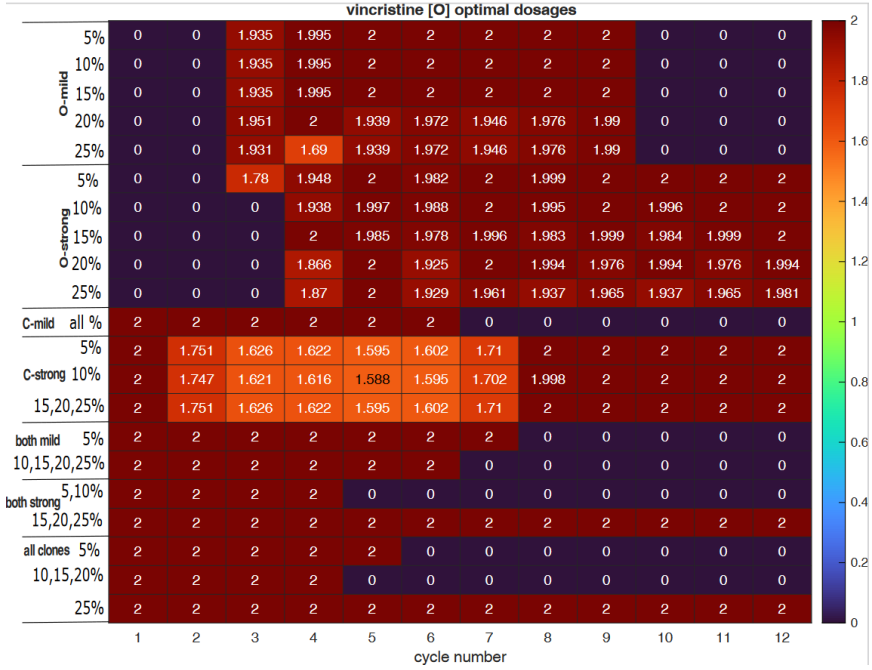

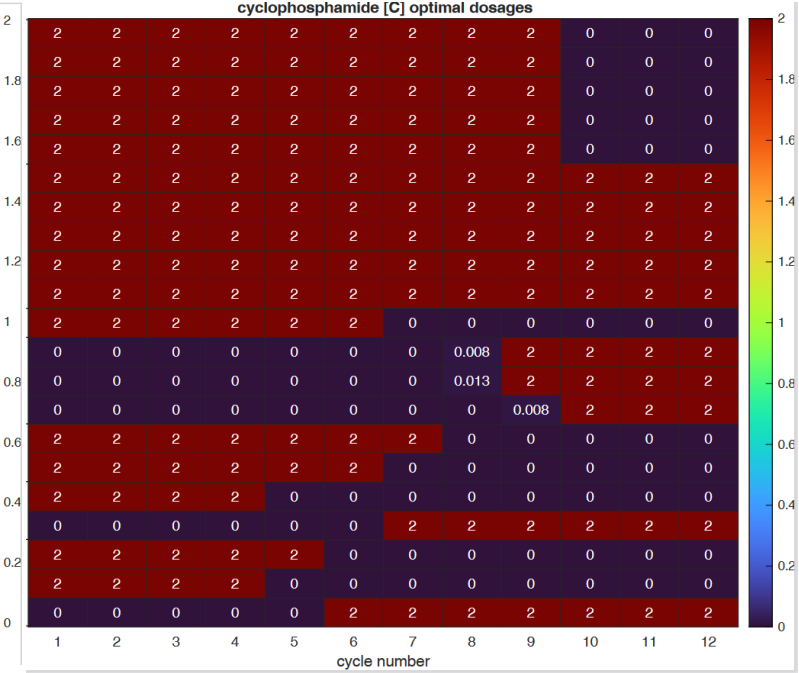

Optimisation

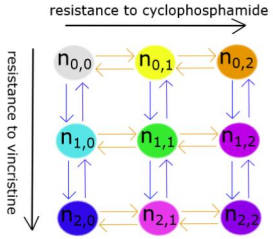

Evolutionary principles.

- Turn some clones against the others.

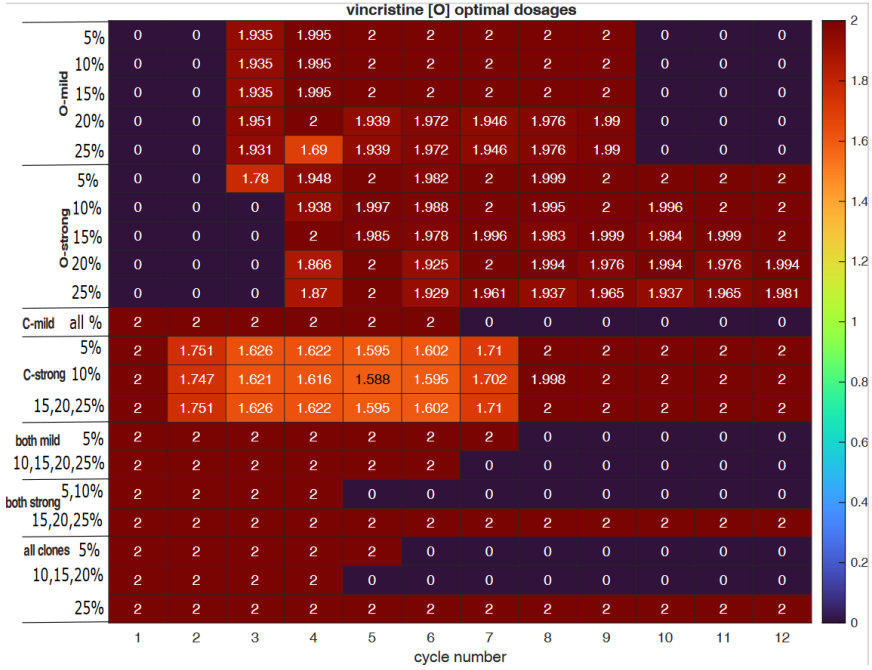

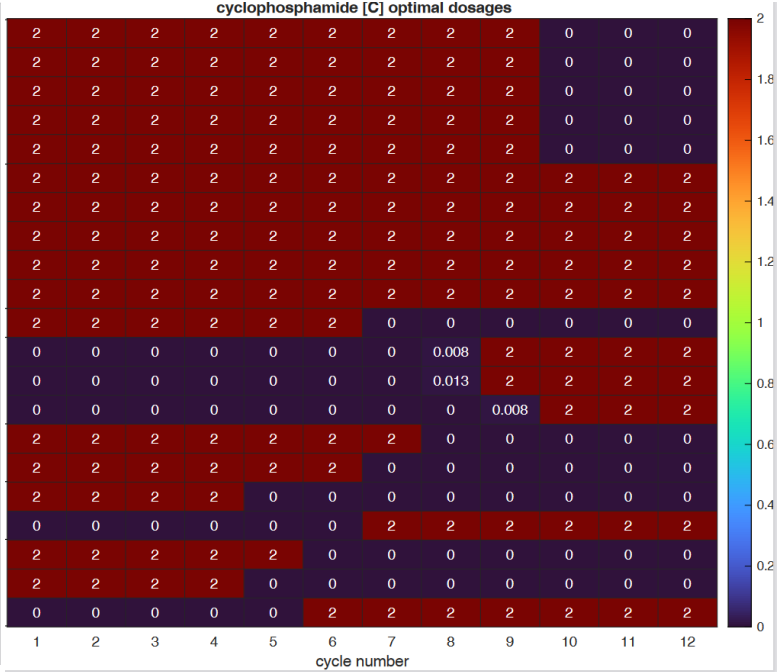

Optimisation

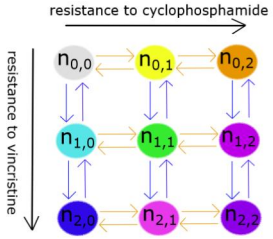

Evolutionary principles.

- Turn some clones against the others.
- Apply drug A only to make the tumour susceptible to drug B before applying drug B.

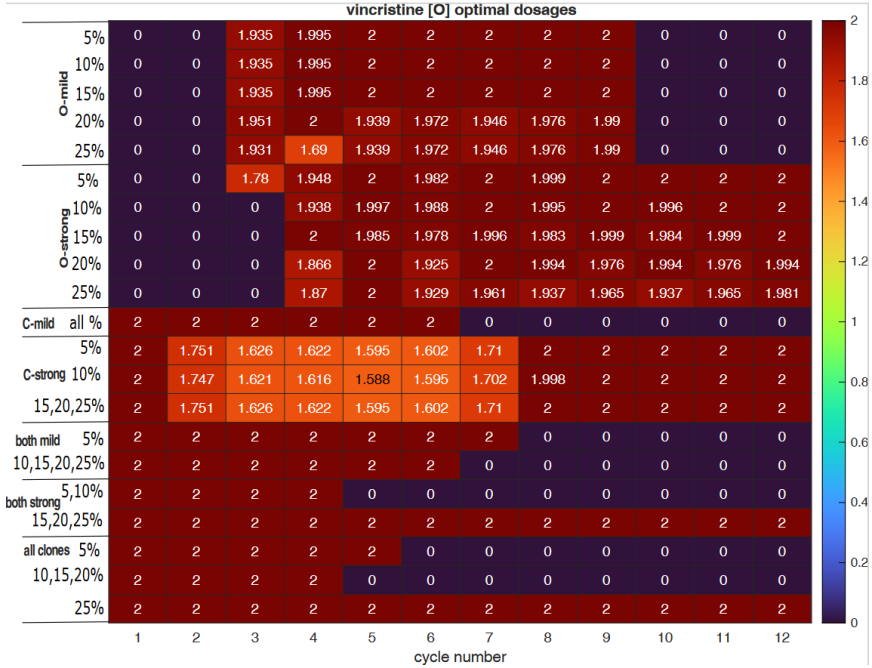

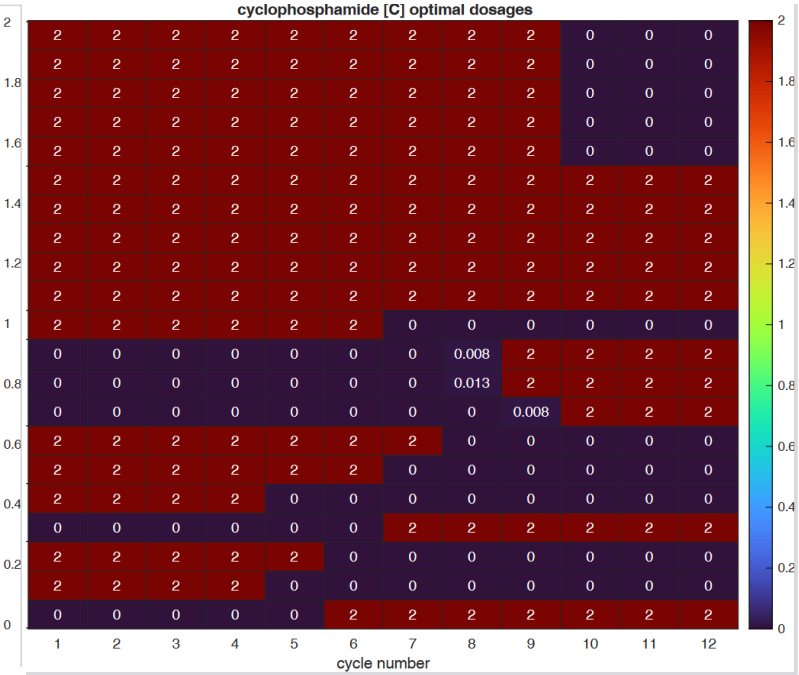

Conclusions

1. Different problems require different modelling frameworks.

2. Gradient descent can calibrate mechanistic models too.

3. Violin plots and heat maps are powerful visualisation tools.

4. Unsupervised learning can extract insights from large-scale simulation results.

5. Supervised learning can predict the outcome of an expensive simulation.

6. Combination therapy and evolutionary principles can potentially improve multi-modal therapy for high-risk neuroblastoma.